Miner Petrol (2010) 99:243–261
DOI 10.1007/s00710-009-0068-z

ORIGINAL PAPER

Structure, mineralogy and dynamics of the lowermost mantle

Reidar G. Trønnes

Received: 21 January 2009 / Accepted: 3 July 2009 / Published online: 22 July 2009

Abstract The 2004-discovery of the post-perovskite transition initiated a vigorous effort in high-pressure, high-temperature mineralogy and mineral physics, seismology and geodynamics aimed at an improved understanding of the structure and dynamics of the D"-zone. The phase transitions in basaltic and peridotitic lithologies under pT-conditions of the lowermost mantle can explain a series of previously enigmatic seismic discontinuities. Some of the other seismic properties of the lowermost mantle are also consistent with the changes in physical properties related to the perovskite (pv) to post-perovskite (ppv) transition. After more than 25 years of seismic tomography, the lowermost mantle structure involving the sub-Pacific and sub-African Large Low Shear-Velocity Provinces (LLSVPs) has become a robust feature. The two large antipodal LLSVPs are surrounded by wide zones of high Vs under the regions characterized by Mesozoic to recent subduction. The D" is further characterized by a negative correlation between shear and bulk sound velocity which could be partly related to an uneven distribution of pv and ppv. Ppv has higher VS and lower V_Φ (bulk sound speed) than pv and may be present in thicker layers in the colder regions of D". Seismic observations and geodynamic modelling indicate relatively steep and sharp boundaries of the 200-500 km thick LLSVPs. These features, as well as independent evidence for their long-term stability, indicate that they are intrinsically denser than the surrounding mantle. Mineral physics data demonstrate that basaltic lithologies are denser than peridotite throughout the lowermost mantle and undergo incremental densification due to the pvppv-transition at slightly shallower levels than peridotite. The density contrasts may facilitate the partial separation and accumulation of basaltic patches and slivers at the margins of the thermochemical piles (LLSVPs). The slopes of these relatively steep margins towards the adjacent horizontal core-mantle boundary (CMB) constitute a curved (concave) thermal boundary layer, favourable for the episodic generation of large mantle plumes. Reconstruction of the original positions of large igneous provinces formed during the last 300 Ma, using a paleomagnetic global reference frame, indicates that nearly all of them erupted above the margins of the LLSVPs. Fe/Mg-partitioning between pv, ppv and ferropericlase (fp) is important for the phase and density relations of the lower mantle. Electronic spin transition of Fe2+ and Fe3+ in the different phases may influence the Fe/Mg-partitioning and the radiative thermal conductivity in the lowermost mantle. The experimental determination of the $K_{D_{pv/fp}}^{Fe/Mg}\left[=(Fe/Mg)_{pv}/(Fe/Mg)_{fp}\right]$ and $K_{D_{ppv/fp}}^{Fe/Mg}$ is technologically challenging. Most studies have found a $K_{D_{pv/fp}}^{Fe/Mg}$ of 0.1-0.3 and a higher Fe/Mg-ratio in ppv than in pv. The experimental temperature is important, with the partitioning approaching unity with increasing temperature. Although charge-coupled substitutions of the trivalent cations Al and Fe^{3+} seem to be important in both pv and ppv (especially in basaltic compositions), the complicating crystal-chemistry effects of these cations are not fully clarified. The two anti-podal thermochemical piles as well as the thin ultra-low velocity zones next to the CMB may represent geochemically enriched reservoirs that have remained largely isolated from the convecting mantle through a major part of Earth history. The existence of such "hidden" reservoirs have previously been suggested in order to account for the imbalance between the inferred

Editorial handling J. Raith

R. G. Trønnes (✉)
Natural History Museum, University of Oslo,
P.O. Box 1172 Blindern,
N-0318 Oslo, Norway
e-mail: r.g.tronnes@nhm.uio.no

composition of the geochemically accessible convecting mantle and the observed heat flow from the Earth and chondritic models for the bulk Earth.

Introduction

Our insights into the structure and dynamics of the deep Earth come from the integration of geophysical observations and geodynamical models with cosmochemical and geochemical data and high-pressure and high-temperature experimental phase relations and mineral physics. Only the combined developments in these fields can bring about substantial progress in deep Earth understanding. This is illustrated by the 2004-discovery of the perovskite (pv) to post-perovskite (ppv) transition in $MgSiO_3$, $(Mg,Fe)SiO_3$, peridotite and basalt, at pT-conditions corresponding to the D″-zone (Murakami et al. 2004; Oganov and Ono 2004; Iitaka et al. 2004; Hirose et al. 2005; Murakami et al. 2005). The crystallographic and elastic properties of the post-perovskite phase can explain important, and previously enigmatic, features of the seismically defined D″-zone. From a seismological point of view, the discovery of the post-perovskite phase transition was long overdue and has prompted a substantial re-vitalization of deep mantle mineral physics and seismology (e.g. Hernlund et al. 2005; Wookey et al. 2005; Hirose 2006; Lay et al. 2006; van der Hilst et al. 2007; Ohta et al. 2008; Irifune and Tsuchiya 2007; Ohtani and Sakai 2008; Shim 2008; Tateno et al. 2009).

The high-pressure mineralogy of the lowermost mantle can be experimentally investigated using the laser-heated diamond anvil cell, combined with in-situ X-ray diffraction and other spectroscopic measurements using high-brightness synchrotron radiation. The technological challenges and the small sample size still represent major limitations for such studies. The derivation of thermodynamic and mineral physical properties by theoretical first principles computations (DFT-modelling) has proven to be a powerful complement to experimental studies (e.g. Oganov and Ono 2004; Iitaka et al. 2004; Wookey et al. 2005; Stølen and Trønnes 2007) The increasing efforts by many different groups, combined with a continuous development of more powerful computers and software systems, may extend the capabilities of this technique to chemically more complex and disordered minerals. The further rapid development is clearly dependent on improved methods and technology in high-pressure experimentation, seismological data collection and processing, as well as in geodynamic modelling. Our working hypotheses for the dynamics of the core-mantle boundary (CMB) region and for Earth evolution are also strongly influenced by existing and new cosmochemical and geochemical data (e.g. Boyet and Carlson 2005, 2006; Caro et al. 2008).

The CMB is the most profound interface within the Earth in terms of contrasts in temperature, material type and physical properties. The density increases from about 5500–9900 kg/m^3 and the temperature increases by more than 1000 K across the 200–300 km thick thermal boundary layer of the D″-zone, from the mantle adiabatic level of about 2600 K to the CMB temperature of 3700–4100 K (e.g. Ono 2008; Tateno et al. 2009). The anomalous seismic properties of the D″ region, in the form of low S-wave velocity gradients and increased scatter in travel times and amplitudes, were recognized already by Bullen (1949). Seismic tomography studies of the lowermost mantle reveal a clear decoupling of the regional S-wave and P-wave velocity variations (e.g. Masters et al. 2000). The S-wave structure of the lowermost 200–500 km is dominated by two large low shear-velocity provinces (LLSVPs) located near the equator, about 180º apart, under the central Pacific and Africa. Between the two LLSVPs are higher S-velocity regions, generally below areas that have experienced subduction throughout the last 300 Ma.

Because the D″ zone has an ill-defined and variable thickness and is characterized by large lateral and vertical variations in temperature, mineralogy, chemistry and material properties, the current usefulness of this term is questionable. By common practice, however, I will use the D″-terminology occasionally throughout this review article. Although the 2004-discovery of the ppv-transition has stimulated rapid progress in understanding of the CMB-region, many uncertainties and unexplained features remain. This article is an attempt to review the early-2009 status concerning the structure, materials and dynamics of the lowermost mantle. With the most profound thermal boundary layer and the strong lateral and vertical gradients, the region must strongly influence mantle dynamics and Earth evolution.

Seismology and geodynamics of the lowermost mantle

Discontinuities

Lay and Helmberger (1983) first discovered discontinuous S-wave increases at an average depth of about 250 km above CMB. Based on the depth variation to this rather ubiquitous S-wave discontinuity that generally correlates with the inferred temperature variation, Sidorin et al. (1999) suggested that it may be related to a solid-solid phase transition with a Clapeyron slope of about 6 MPa/K. Several studies have later revealed additional weaker and reverse S-wave discontinuites, involving decreasing velocities 50–100 km above the CMB (e.g. Thomas et al. 2004a, b; Lay et al. 2006; van der Hilst et al. 2007). The discovery that the exothermic pv- to ppv-transition has a remarkably large

and positive dp/dT-slope, led Hernlund et al. (2005) to suggest that the very large thermal gradients next to the CMB lead to re-stabilization of the high-entropy phase pv next to the CMB (Fig. 1). Lateral temperature variations between different regions of the D″-zone, will lead to variable thickness of the ppv-layer. Detailed mapping of the upper (V_S-increase) and lower (V_S-decrease) discontinuities beneath Central America, revealing a 140 km vertical step on the upper discontinuity, has been interpreted as the folding and flattening of a vertically descending subducted slab at the CMB (Hutko et al. 2006).

S-wave anomalies, LLSVP

The large-scale S-wave velocity structure of the lowermost mantle, involving the Pacific and African LLSVPs and high velocities in the surrounding regions, has been recognized since the earliest seismic tomography compilations (e.g. Dziewonski and Anderson 1984). The two equatorial or slightly sub-equatorial LLSVPs, located 180° apart, coincide with the two main geoid highs and supposedly also with concentrations of intraplate volcanic centres or hotspots (e.g. Anderson 1982; Richards and Hager 1984). The approximate outlines of the LLSVPs are shown in Fig. 2. The lowermost mantle velocity structure is reproducible in a wide range of tomographic S-wave models (compilations by e.g. Masters et al. 2000; Montelli et al. 2006; Ritsema 2005). Even the shapes of the two LLSVPs

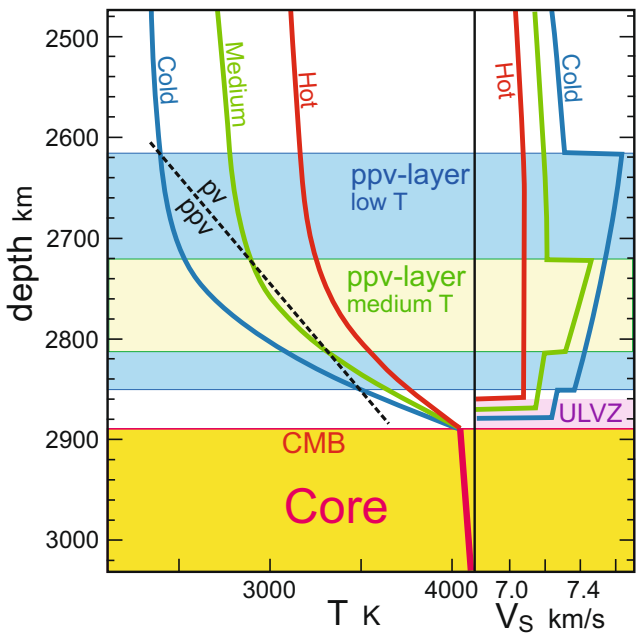

Fig. 1 The double-crossing scenario for the pv-ppv-transition, as first suggested by Hernlund et al. (2005). Left panel: depth versus T with three different geotherms (hot, medium and cold) and the pv-ppv-transition boundary. Right panel: resulting S-wave model. ULVZ: Ultra-low velocity zone

are largely reproduced in most of the models. The amplitudes of the S-velocity variation of the lowermost 200–400 km of the mantle (and the uppermost 100–300 km) are considerably larger than the variation in the upper and middle part of the lower mantle (Masters et al. 2000; Montelli et al. 2006; Ritsema 2005) with perturbation from average S-velocity in the lowermost mantle covering a total range of 4–6%.

An enigmatic feature of the seismic properties of the lowermost mantle is a clear anti-correlation between the S-wave speed and the bulk sound speed of the lowermost mantle ($V_S^2 = G/r$ and $V_\Phi^2 = K/\rho$, where G, K and ρ are shear modulus, bulk modulus and density, respectively) (e.g. Masters et al. 2000). The global map of the bulk sound velocity of the D″-zone has high V_Φ coinciding with the LLSVPs and low V_Φ corresponding to the surrounding high V_S areas.

Geodynamics of LLSVP

It is difficult to account for the large S-velocity anomalies in the lowermost mantle in a purely isochemical mantle (e.g. McNamara and Zhong 2005). The geographical correspondence between the negative S-velocity anomalies and overlying geoid highs, the distribution of surface volcanic centres and the Mesozoic history of subduction has been discussed by several authors (Anderson 1982; Richards and Engebretson 1992; Richards et al. 1997). The interpretation of the LLSVPs as so-called superplumes or thermochemical plumes has been supported by fluid dynamics experiments and numerical models (e.g. Forte and Mitrovica 2001; Davaille et al. 2002, 2005). The underlying assumption in these models is that the LLSVPs have elevated intrinsic density relative to the surrounding mantle, but insufficient density contrast to prevent intermittent thermal buoyancy if heated by a lower thermal boundary layer. Davaille et al. (2005) interpret the evolution of the African LLSVP or thermochemical plume in the context of Pangea evolution and break-up and the emplacement of Large Igneous Provinces (LIPs) with associated plume tracks. A key concept in this interpretation is that the thermochemical "superplume" itself develops intermittent thermal instabilities that rise to the lithosphere to create LIPs and plume tracks.

The creation of the two LLSVPs, 180° apart and centred near but slightly to the south of the equator, by convective sweeping of chemically denser material in the lowermost mantle can be roughly modelled by imposed downwelling under the recent to present subduction zones (e.g. McNamara and Zhong 2005). Therefore, the spatial relationships between the LLSVPs, recent subduction zones and the geoid seem to be a natural consequence of global mantle dynamics. As discussed by Richards et al. (1997) and Steinberger and Torsvik (2008), the associated mass distribution must be linked to the orientation of the Earth rotation axis and continuously adjusted via true polar wander.

An important discovery was made by Burke and Torsvik (2004), who restored the LIPs spanning the last 250 Ma to their original eruption sites in a global paleomagnetic reference frame. Most of the LIPs were relocated to positions that lie roughly above the margins of the LLSVPs, with the great majority clustering around the African LLSVP (Fig. 2). Further refinement and testing of this spatial and temporal association, using a range of different S-wave tomographic models and paleomagnetic relocation frames (Torsvik et al. 2006, 2008a, b; Burke et al. 2008) have provided a strong case for episodic plume generation along the LLSVP margins. The statistically documented non-randomness of the connection between the peripheries of the *currently* imaged LLSVP and the restored LIP positions puts important constraints on the long-term stability of these provinces. Because strong heating from below at the CMB would generally induce thermal expansion and buoyancy, a significant compositional density contrast between the LLSVP-material and surrounding mantle is required. Therefore, the expression "thermo-chemical pile" seems appropriate for the LLSVP-material.

The thickness variation of the thermochemical piles is not well defined. Because the horizontal velocity contrasts increase downwards, the outlines are best defined just above the CMB. Burke et al. (2008) estimate that the African and Pacific thermo-chemical piles represent 1.13 and 0.79 wt % of the total mantle, respectively. The sharpness and steepness of the LLSVP-margins have been investigated in several detailed seismic studies covering specific areas (reviewed by Garnero et al. 2007). The southern half of the African LLSVP-periphery is the portion where sharp and steep boundaries are best documented. This is also the region where about 10 LIPs were formed successively during the 182–65 Ma period (e.g. Torsvik et al. 2006).

The condition for stability of rather steep margins and large thickness is that the density contrast is moderate. Density contrasts of 2–5% seem appropriate to generate the thermochemical piles (McNamara and Zhong 2005; Garnero and McNamara 2008). Increasing the density contrast significantly makes the piles flatter. An important condition for steep and sharp pile margins may also be that the dense material has higher bulk modulus at CMB-pressures than the surrounding mantle. The stabilization of a semi-vertical pile boundary will be aided by greater volume decrease (density increase) of the surrounding mantle, relative to the pile material, upon downwards pressurization towards the CMB.

ULVZ and seismic anisotropy

In addition to the large lateral and vertical gradients in temperature and physical properties, portions of the CMB-

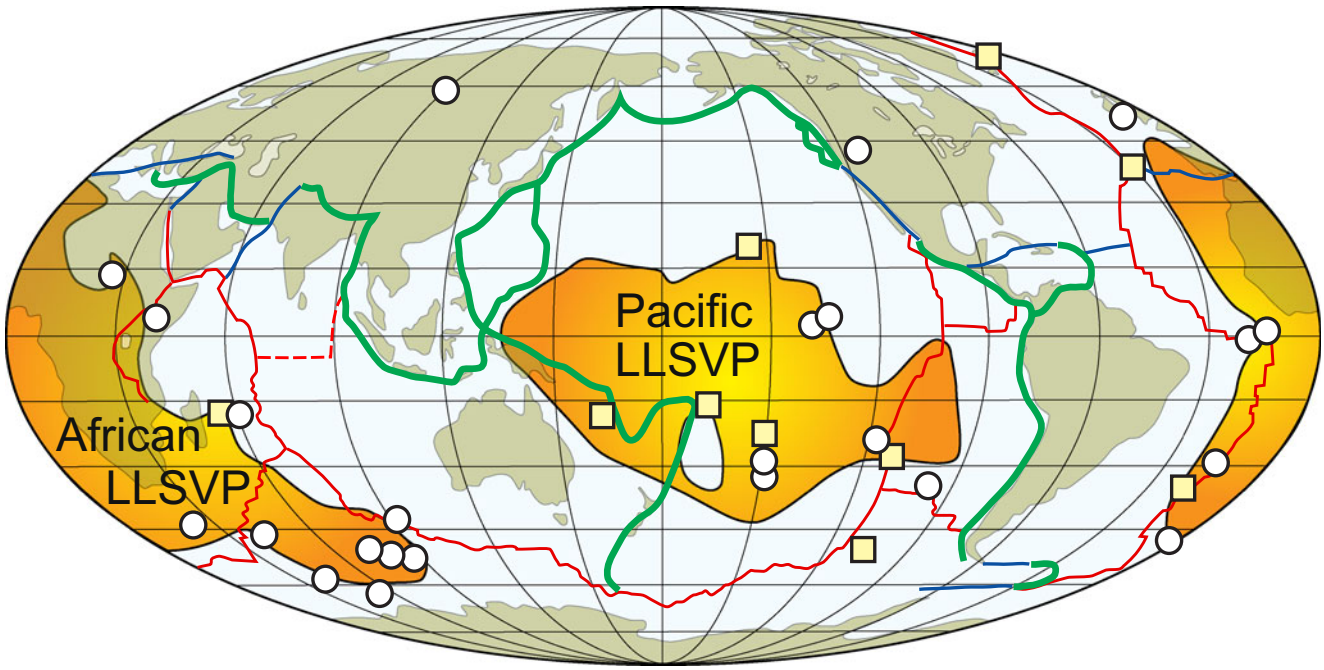

Fig. 2 Simplified global map showing the distribution of the antipodal Large Low-Shear-Velocity Provinces (LLSVP). The outline of the provinces are based on the SMEAN shear wave velocity anomaly model for 2800 km depth of Becker and Boschi (2002). Circles represent 24 LIP-sites, restored to their original eruption locations with respect to a global paleomagnetic reference frame. Squares are the positions of 10 mantle plumes of deep origin, identified by Montelli et al. (2006). The figure is considerably changed, but largely based on Fig. 6 of Torsvik et al. (2006). The two LIP-sites that are furthest removed from the outlined LLSVPs, i.e. the Columbia River Province (14 Ma) and the Siberian Traps (251 Ma), both seem to be spatially associated with velocity gradients and minor LSVPs not shown in this figure (Burke et al. 2008; Torsvik et al. 2008a, b)

region are characterized by areas with 10–40 km thick ultra-low-velocity zones (ULVZ) directly above the CMB (e.g. Lay et al. 1998, 2004; Lay 2005). The ULVZ areas have P- and S-wave velocity reductions of up to 10 and 30%, respectively, probably caused by partially molten silicate material. Suggestions that the ULVZ could be related to extra dense solid material have also been made by Dobson and Brodholt (2005) and Mao et al. (2006). The mapping of the CMB-area with ULVZ is not complete, with less than 50% of the CMB-surface mapped (Lay 2005). The ULVZ are absent in about two thirds of the investigated area, primarily outside the LLSVP-regions, and present in about one third of the area, largely inside the LLSVPs. Numerical modelling of the convection regime associated with the generation and stabilization of the thermochemical piles indicates that the pile-margins would be favourable locations for ULVZ-accumulation (Garnero et al 2007; Labrosse et al 2007). A few recent high-resolution studies of the ULVZ structure near the edge of the Pacific LLSVP support these results (Rost et al. 2005; Lay et al. 2006).

The D″-zone is also characterized by a strong S-wave splitting with SH (horizontally polarized S-wave) faster than SV in the regions characterized by positive V_S-perturbations, i.e. in the areas outside the LLSVPs (e.g. Wookey and Kendall 2007). Although the crystallographic mechanism for the anisotropic behaviour is still uncertain, ppv appears to be a better causative candidate for the lowermost mantle anisotropy than pv (Wookey et al. 2005; Maupin et al. 2005; Wookey and Kendall 2007; Shim 2008). Ppv with a [100](010) slip system seems to be the most likely candidate. Anisotropic contributions from the weaker mineral, ferropericlase, are also rather likely (e.g. Yamazaki et al. 2006). The high SH/SV-ratio in the D″ zone in areas underlying the locations of Mesozoic to recent subduction zones may be interpreted as the result of horizontal flow above the CMB of cold material from the zones of major downwelling under Australia, Asia, North and South America and Antarctica (i.e. the areas surrounding the LLSVPs, Fig. 2).

Crystallography, mineral physics and phase relations of pv and ppv

The crystal structures of pv (space group Pbnm) and ppv (Cmcm) are shown in Fig. 3. Whereas the SiO_6^{8-}-octahedra are corner-linked in 3 dimensions in the pv-structure, they are edge-linked along the a-axis in the ppv-structure, leading to rigid ac-layers and a longer and more compressible b-axis-dimension. Single-crystal structure refinements by XRD and single crystal elasticity measurements on $MgSiO_3$-ppv are practically impossible because the structure is not quenchable to ambient conditions. Experimental bulk modulus measurements combined with computational mineral physics to obtain both bulk (K) and shear (G) modulus for the $MgSiO_3$-polymorphs (e.g. Wookey et al. 2005; Stackhouse et al. 2005a, b) have established that the pv-ppv transition involves a decrease in K and increase in G. Such an anti-correlation between ΔK and ΔG is unusual for an isochemical first-order phase transition but may in this case contribute to the observed anti-correlation between V_S and V_Φ in the D″-region (e.g. Wookey et al. 2005; Stølen and Trønnes 2007).

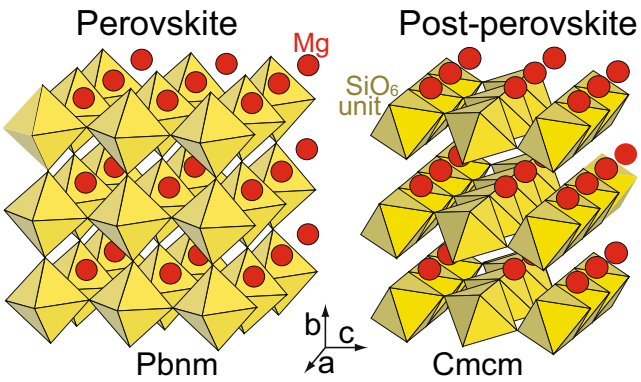

Fig. 3 Simplified sketch of the crystal structures of pv (space group Pbnm) and ppv (space group Cmcm)

Similar relationships between bulk and shear moduli in pv and ppv were observed for the analogue composition $CaIrO_3$, for which both of the polymorphs can be synthesised as large single crystals in the piston cylinder apparatus. The compressibility curves for the $CaIrO_3$-polymorphs determined by single crystal DAC-experiments (Boffa-Ballaran et al. 2007) and DFT-computations (Stølen and Trønnes 2007) demonstrate that the excessive compressibility of ppv is caused by the large b-axis compression (Fig. 4). The a- and c-axes are less compressible in ppv than in pv.

The DFT-modelling by Caracas and Cohen (2005) and Tsuchiya and Tsuchiya (2006) for the pv- to ppv-transition in $MgSiO_3$, $FeSiO_3$ and Al_2O_3 indicate that ΔG and ΔK for $MgSiO_3$ are positive and close to zero, respectively, and that increasing proportions of the $FeSiO_3$ and Al_2O_3 components lead to decreasing values of both ΔG and ΔK. In basaltic compositions, therefore, even the shear-wave velocity may drop at the pv- to ppv-boundary.

Experimental studies of the equations of state for pv and ppv of compositions $MgSiO_3$, $Mg_{0.9}Fe_{0.1}SiO_3$, and $Mg_{0.85}Fe_{0.15}Al_{0.15}Si_{0.85}O_3$ at 100–160 GPa indicate that V_Φ decreases across the pv- to ppv-transition and that the incorporation of the $FeSiO_3$- and $FeAlO_3$-components decreases V_Φ in both of the phases (Guignot et al. 2007; Lundin et al. 2008; Nishio-Hamane et al. 2008; Nishio-Hamane and Yagi 2009). The pv- to ppv-transition in pure

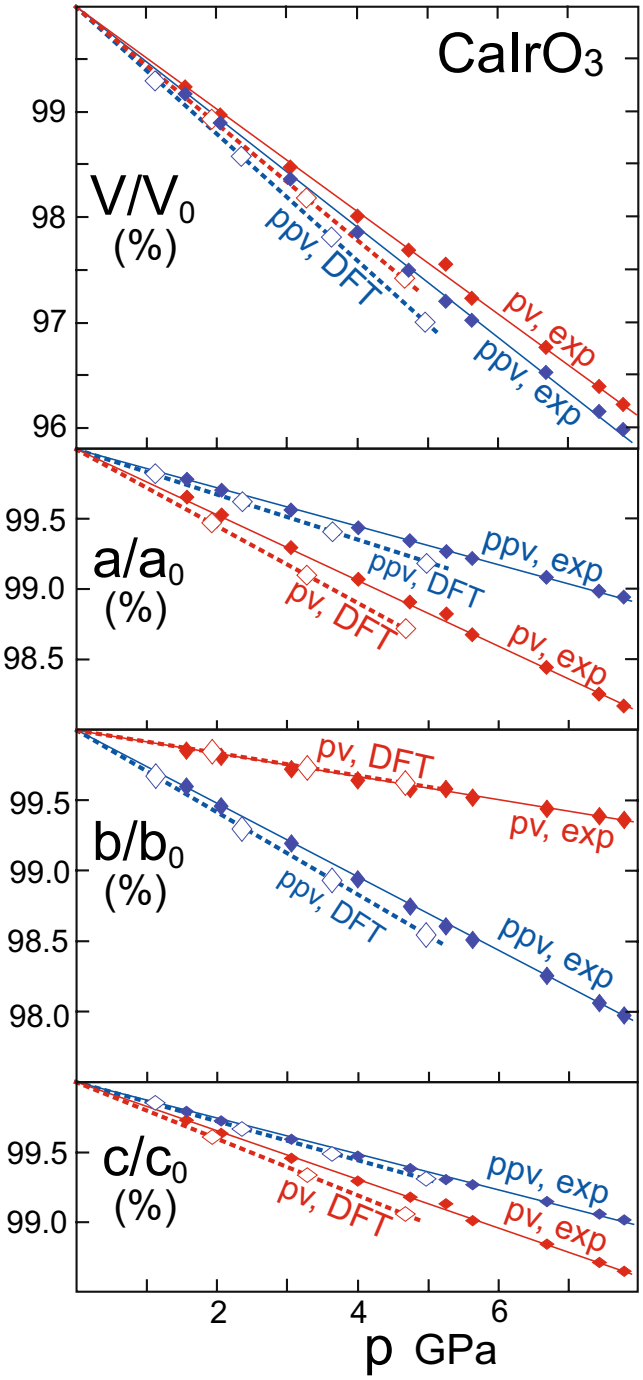

Fig. 4 Compressibility curves for $CaIrO_3$-pv and -ppv. Filled symbols connected with continuous lines represent experimental data from in-situ single-crystal XRD in methanol-ethanol pressure medium in the diamond anvil cell (Boffa-Ballaran et al. 2007) and open symbols connected with thicker, dotted lines are based on Density Functional Theory (DFT) computations (Stølen and Trønnes 2007)

$MgSiO_3$ would result in a 3.5% decrease in V_Φ. The incorporation of about 15% of either the $FeSiO_3$-component or the $FeAlO_3$-component would lead to a decrease of V_Φ of approximately 2.2–2.5% in each of the two phases.

The pv- to ppv-transition involves a small decrease in volume (about 1%) and a large decrease in entropy, corresponding to a very large and positive Clapeyron slope ($dp/dT = \Delta S/\Delta V$) of 13.3 MPa/K for $MgSiO_3$ (Tateno et al. 2009). Based on the topography of the main D″-discontinuity, Sidorin et al. (1999) originally predicted a slope of 6 MPa/K for a hypothetical phase transition, and the first DFT-modelling results of the pv-ppv-transition in $MgSiO_3$ gave dp/dT-slopes of 8-10 MPa/K (Oganov and Ono 2004; Tsuchiya et al. 2004). The slope of 13.3±1.0 MPa/K, based on a careful LH-DAC-investigation with MgO as internal pressure standard, is more than three times steeper than the slopes of the phase transitions in the upper mantle and transition zone.

Mineralogy and density of basaltic and peridotitic material

Mineral proportions

The phase relations, mineral proportions and density relations of basaltic and peridotitic lithologies within the perovskite stability range in the central parts of the lower mantle were investigated experimentally by Kesson et al (1998); Hirose et al. (1999) and Ono et al. (2001). After the discovery of the post-perovskite phase transition for composition $MgSiO_3$, a number of new experimental studies have focussed on phase relations, element partitioning and mineral physics of peridotitic and basaltic materials in the lowermost mantle pressure range (e.g. Murakami et al. 2005; Hirose et al. 2005; Ono et al. 2005a, b). The approximate mineral proportions are summarized in Fig. 5. At a depth of 2000 km (about 87 GPa), the peridotite (pyrolite) composition contains 70% Mg-perovskite (pv), 20% ferropericlase (fp) and 10% Ca-perovskite (Ca-pv) and the basalt (MORB) composition includes 40% pv, 22% Ca-pv, 18% Ca-ferrite-structured NaAl-rich phase (NAL) and 20% $CaCl_2$-structured silica. Moving into the stability range of post-perovskite (ppv), in the lowermost mantle the proportions of fp and Ca-pv in a pyrolitic composition remain almost unchanged. The post-perovskite transition in a basaltic composition, however, is accompanied by a phase transition from the $CaCl_2$-phase to a α-PbO_2-structured silica-dominated phase at overlapping pT-conditions. These transitions are associated with decreasing proportion of the NAL-phase because the Al-content in the α-PbO_2- and the Na-contents of post-pv-phases are considerably higher that those in the $CaCl_2$-phase and pv, respectively (Hirose et al. 2005).

Density relations

Figure 6 illustrates the densities of the major mineral end member components along a lower mantle adiabat from

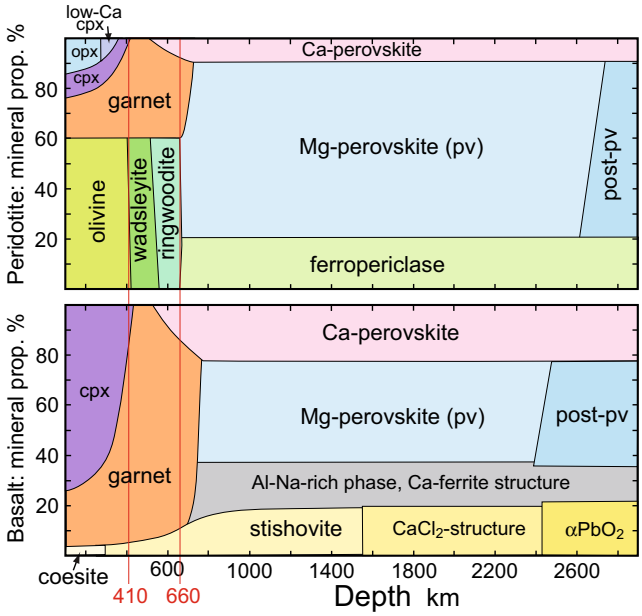

Fig. 5 Approximate mineral proportions in peridotite (pyrolite) and basalt (MORB) compositions as a function of mantle depth. Based on Irifune and Tsuchiya (2007) and Hirose et al. (2005)

Irifune and Tsuchiya (2007). Based on the lower mantle mineral proportions and the density-pressure curve of each mineral, they calculated the density-pressure curve for pyrolitic, harzburgitic and basaltic compositions along the lower mantle adiabat. The three curves are sub-parallel in the 60–110 GPa range (at pressures below the basaltic densifications caused by the SiO_2- and pv-ppv-transitions), with the pyrolite curve overlapping with the PREM-model. The harzburgite curve lies less than 20 kg/m^3 below and the MORB-curve is about 50 kg/m^3 higher than the pyrolite and PREM-curves. Hirose et al. (2005) and Hirose (2006) estimated slightly larger density differences of at least 100 kg/m^3 between basaltic compositions and PREM and indicate a weak incremental densification of MORB relative to the PREM-model in the 60–110 GPa range.

The density-pressure curves of basaltic and peridotitic materials are sub-parallel in spite of the rather wide range of bulk moduli for the different minerals (Fig. 6). The two phases that differ the most are the relatively compressible fp and the relatively incompressible silica-phases. Because the stishovite to $CaCl_2$-structure is a second order phase transition, it is largely invisible in terms of the density-pressure curve.

Hirose et al. (2005) found that the increased Al-partitioning into the α-PbO_2-structured silica phase may cause a density reduction contribution due to the $CaCl_2$ to α-PbO_2 transition. The density increase associated with this transition in Fig. 6 is based on Irifune and Tsuchiya (2007). However, Fig. 6 shows a transition pressure of about 115 GPa, in accordance with the recent study of Ohta et al. (2008).

Crystal chemistry and Fe/Mg-partitioning in pv and ppv

The partial edge-linking of the SiO_6^{8-}-octahedra in ppv results in suboptimal shielding of the highly charged Si^{4+}-cations by O^{2-}-anions (e.g Shim 2008). The problem of inadequate shielding would be partly alleviated in a ppv-structure with trivalent substitutional components, e.g. the charge-coupled components Al_2O_3, Fe_2O_3 and $FeAlO_3$ or the O-defect component $MgAlO_{2.5}$. Therefore, one might expect strong tendencies for such substitution in ppv. There is currently considerable uncertainty with respect to the solubility of the trivalent cation components in pv and ppv of the lowermost mantle.

Perovskite

The solubility of the Al_2O_3-component in $MgSiO_3$-based perovskites synthesized at 40–80 GPa and 2000–2600 K is about 25 mol% (Walter et al. 2004, 2006). The $MgSiO_3$-based pv-structure can accommodate a similar proportion of the components Fe_2O_3 (Andrault and Bolfan-Casanova 2001) and $FeAlO_3$ (Nishio-Hamane et al. 2005) at pressures of 50–60 GPa. The studies by Nishio-Hamane et al. (2005) and Vanpeteghem et al. (2006) indicate that Fe^{3+} and Al^{3+} prefer the cubic and octahedral perovskite sites, respectively. The O-defect substitution mechanism, e.g. in the form of the $MgAlO_{2.5}$-component, seems to be of minor importance in the lower mantle (Walter et al. 2006).

The experiments on a natural basaltic composition by Ono et al. (2001) at 30–37 GPa indicate that the total proportions of the Al_2O_3-, Fe_2O_3- and $FeAlO_3$-components are 25–33 mol%, based on a charge-balancing of the mineral formulas. The perovskites have Fe^{3+}/Fe_{total}-ratios

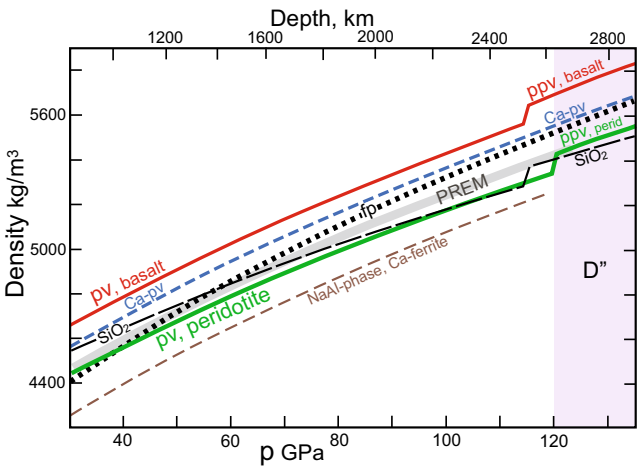

Fig. 6 Density-pressure curves for the main lower mantle minerals. Slightly modified from Irifune and Tsuchiya (2007)

of 0.66–0.71, whereas the majoritic garnet crystallized from the same composition at 25 GPa has a Fe^{3+}/Fe_{total}-ratio of 0.27, with 22 mol% combined trivalent substitution. Various studies, e.g. Frost et al. (2004), indicate that the Fe^{3+}-incorporation in perovskite is largely independent of oxygen fugacity and facilitated by a substantial Al-content.

Post-perovskite

Ab initio computations by Oganov and Ono (2005) indicate that Al_2O_3 adopts the ppv-structure ($CaIrO_3$-type) above 130 GPa. Tateno et al. (2005) investigated the pyrope composition (25 mol% Al_2O_3) experimentally at about 2000 K (1600–2400 K) and 120–180 GPa and found that pv is stable to about 140 GPa, followed by a two-phase region at 140–150 GPa, and a single phase ppv at 170–180 GPa. The pv-ppv-transition for $MgSiO_3$ occurs at about 115 GPa and 2000 K (Tateno et al. 2009) and the higher transition pressure recorded for the pyrope composition indicates that pure Al_2O_3-substitution expands the stability field of pv. Experimental studies of pure Fe_2O_3 indicate a phase transition from the orthorombic pv-structure (Rh_2O_3-II-type) to the ppv-structure ($CaIrO_3$-type) at 60–70 GPa and about 2000 K (Ono and Ohishi 2005; Shim et al. 2009). The stabilization of Fe_2O_3-based ppv at relatively low pressure might indicate that the substitution of ferric iron in ppv is favourable.

DFT-modelling by Akber-Knutson et al. (2005) and Zhang and Oganov (2006a, b) shows that the O-defect substitution (e.g. the $MgAlO_{2.5}$-component) is energetically less favourable than the charge-coupled substitutions of trivalent cations like Al and Fe^{3+}. The ppv-structure seems to be able to accommodate large proportions of ferrous iron as the $FeSiO_3$-component (Caracas and Cohen 2005; Mao et al. 2005).

Aluminous and iron-rich ppv crystallized in basaltic compositions has high proportions of Fe^{3+}. The ppv formed in a MORB-composition at 113 GPa and 2240 K has an average $Fe^{3+}/\Sigma Fe$-ratio of 0.65 (Hirose et al. 2005; Sinmyo et al. 2006). The ppv in this bulk composition has also a remarkably high Na-content (2-cation formula based on data in Hirose (2005): $Na_{0.17}Ca_{0.02}Fe^{2+}_{0.12}Mg_{0.52}Fe^{3+}_{0.23}Al_{0.25}Ti_{0.04}Si_{0.65}$). Some of the trivalent A-site substitution may therefore be compensated by A-site Na, without affecting the B-site. The possible presence of O-defects or protons may complicate these matters.

Al-free ppv in the system MgO-FeO-SiO_2 has $Fe^{3+}/\Sigma Fe$-ratios of only 0.1–0.2 (Sinmyo et al. 2008). The starting material gels of Sinmyo et al. (2006, 2008) were dehydrated under identical conditions of 1273 K and oxygen fugacity slightly above the iron-wustite-buffer and should accordingly have the same proportion of Fe^{3+} (10–20% of total Fe). Therefore, the high proportion of Fe^{3+} in the aluminous composition suggests an essential role for the coupled Al-Fe^{3+}-substitution.

The partitioning of Fe^{3+}, Fe^{2+}, Mg, and Al between pv, ppv and fp in peridotitic and basaltic material associated with the pv-ppv-transition will largely influence density relations across the phase boundary, and may therefore partly control the dynamics of the D″ region. Recently, several experimental studies, directly or indirectly addressing the element partitioning, have given somewhat conflicting results. The solubility levels of trivalent cations in both pv and ppv in a basaltic compositions can be extracted from the study of Hirose et al. (2005). The pv crystallized at 60 GPa (along with Ca-pv, stishovite and a Ca-ferrite-structured NaAl-rich phase) has subequal amounts of Fe^{3+} and Fe^{2+} and about 20 mol% trivalent substitution components and insignificant Na-content. In contrast, the ppv crystallized at 113 GPa has slightly higher Fe- and Ti-content, higher Fe/Mg, lower Al-content and a very high Na-content (5 wt% Na_2O). Charge-balancing of the resulting mineral formula requires 100% Fe^{3+} and additional O-vacancies.

Fe/Mg-partitioning, pv-ppv-fp

The total Fe/Mg-ratios of pv (at 60 GPa) and ppv (at 113 GPa) from the experimental study of a basaltic composition by Hirose et al. (2005) are 0.52 and 0.67, respectively. In a similar experimental investigation of a peridotite composition (pyrolite) by Murakami et al. (2005), the opposite variation was recorded, with total Fe/Mg-ratios of pv (at 92 GPa) and ppv (at 124 GPa) of 0.05 and 0.02, respectively.

Such conflicting results are also seen in the Fe/Mg exchange partitioning coefficients for the pv/fp and ppv/fp pairs [e.g. $K_D^{Fe/Mg} = (Fe/Mg)_{pv} \big/ (Fe/Mg)_{fp}$]. The preferential partitioning of total iron into ppv, relative to pv, expressed by higher $K_D^{Fe/Mg}(ppv/fp)$ than $K_D^{Fe/Mg}(pv/fp)$, was seen in experimental studies on San Carlos olivine composition (Fo88) by Kobayashi et al. (2005) and Auzende et al. (2008). In these studies, the $K_D^{Fe/Mg}$ increased from 0.10–0.25 for the pv-fp partitioning to 0.3–0.65 for the ppv-fp partitioning. Although the nominal composition involved only ferrous iron, Auzende et al. (2008) documented considerable redox disproportionation of Fe^{2+} to observed Fe-metal nanodroplets in the perovskite. Based on the Fe/Mg ratios in the run product phases compared to the starting material composition, they calculated that the Fe-loss to the metal phase varied between 30% and 48% for the pv-experiments and 9% for the ppv-experiment. A considerable proportion of ferric iron may therefore be present in pv and ppv in all of these experiments.

Sinmyo et al. (2008) discussed the problems with strong Soret diffusion of Fe away from the central part of the laser-heated hot spot and concluded that the $K_D^{Fe/Mg}$ for the pv/fp-

and ppv/fp-partitioning is rather constant at 0.2–0.3 throughout the lower mantle pressure range within the limited temperature range of 2000–2500 K, corresponding to the lower mantle adiabat. The $K_D^{Fe/Mg}$ increases towards unity with increasing temperature (estimated to 0.4–0.5 at 3000 K).

The LA-DAC experiments by Mao et al. (2004, 2005), however, resulted in a strong Fe-partitioning into ppv, relative to pv. Mao et al. (2004) investigated two synthetic Ca-free orthopyroxenes (En80 and En60) and San Carlos olivine (Fo88) at 2000–2500 K and recorded an approximate phase loop between pv-En90 and ppv-En60 at about 100 GPa and between pv-En94 and ppv-En75 at about 110 GPa. Mao et al. (2005) synthesized single-phase ppv from orthopyroxene starting materials in the compositional range En80-En20 at 120–150 GPa and 2000 K, indicating large solubility of the $FeSiO_3$-component in ppv. Experiment on a pure $FeSiO_3$-composition, however, resulted in mixed oxides.

Phase relations of basaltic and peridotitic compositions at D″-conditions — Seismologic and geodynamic implications

Phase relations and seismic velocities

The experimental studies of Mao et al. (2004); Hirose et al. (2005); Murakami et al. (2005) and Ono et al. (2005) address the phase relations associated with the pv-ppv-transition in a range of compositions with variable Fe/Mg-ratios. The results are summarized by e.g. Hirose (2006) but are still somewhat inconclusive, in terms of the exact pT-condition and Clapeyron slope of the transition. As pointed out by Hirose (2006), alternative equations of state for a variety of internal pressure calibrants is a major source of uncertainty. Recent contributions by Tateno et al. (2009) on the exact location and Clapeyron slope of the $MgSiO_3$ phase boundary and by Ohta et al. (2008) on a redetermination of the pyrolite and MORB phase boundaries are attempts to clarify the situation. The phase boundaries from these two studies are shown in Fig. 7. The overall agreement with the information compiled by Hirose (2006) is generally good. However, Tateno et al. (2009) find a considerably larger Clapeyron slope of 13.3 MPa/K for the $MgSiO_3$ phase boundary. As expected from the overall Fe/Mg-partitioning results referred to above, the pv-ppv-transition occurs at lower pressure in the Fe-rich MORB composition compared to the pyrolite and $MgSiO_3$ compositions. Predicted phase relations in the simple binary system $MgSiO_3$-$FeSiO_3$ were presented in the recent reviews by Irifune and Tsuchiya (2007) and Ohtani and Sakai (2008). Fig. 8 is a suggested modification of these

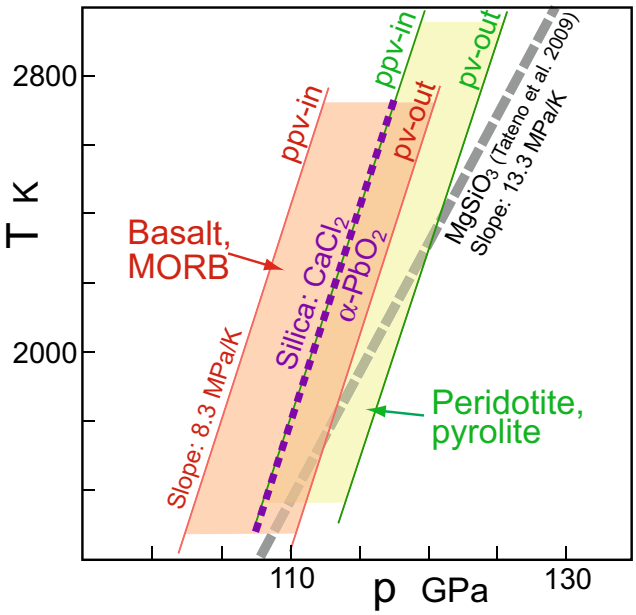

Fig. 7 The stability range of pv and ppv in basalt (MORB) and peridotite (pyrolite) compositions and the $CaCl_2$-αPbO_2-transition of the silica-dominated phase (in basaltic material) determined by Ohta et al. (2008). The thick stippled line is the pv-ppv-phase boundary for $MgSiO_3$ determined by Tateno et al. (2009)

two different binary phase diagrams, drawn to be more consistent with the combined evidence referred to above. The suggested pv-ppv phase loop in Fig. 8 is considerably narrower than that presented by Mao et al. (2004).

A wide pv-ppv phase loop in the enstatite-ferrosilite system is in apparent conflict with relatively sharp seismic

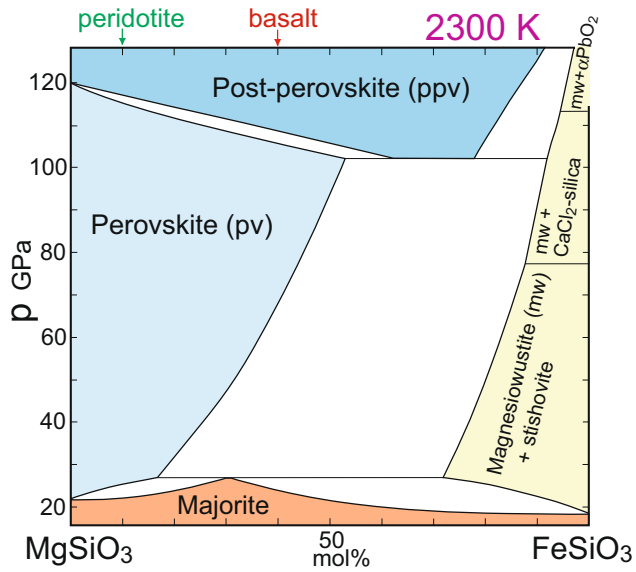

Fig. 8 Predicted and schematic phase relations in the systems enstatite-ferrosilite at 20–120 GPa and a temperature of about 2300 K. Partly based on Irifune and Tsuchiya (2007) and Ohtani and Sakai (2008), but modified to be largely consistent with the various studies discussed in the main text

discontinuities. It is possible, however, that the presence of considerable proportions of ferric iron and/or aluminum in a ternary or quaternary system would increase the stability of both pv and ppv and thereby reduce the width of the binary phase loop. Some studies dealing with the 410 km discontinuity have discussed various mechanisms by which a seismic discontinuity can appear sharper than indicated by the binary phase loop involving the main transforming phases (Helffrich and Wood 1996; Stixrude 1997; Frost 2003).

As documented by Hirose et al. (2005) and Ohta et al. (2008), the pv-ppv-transition in the MORB-composition corresponds closely to the phase transition of the silica-dominated phase from $CaCl_2$- to α-PbO_2-structure in pT-space. Ohta et al. (2008) emphasize the important geophysical and geodynamical implications of this coincidence. The observations that the shear wave velocity of ppv decreases considerably with increasing Fe/Mg-ratio and Al-content (Caracas and Cohen 2005; Tsuchiya and Tsuchiya 2006) indicate that the S-velocity may drop at the pv-ppv-transition in basaltic lithologies. The silica-phase transition from the $CaCl_2$- to the α-PbO_2-structure will probably also result in S-velocity decrease (1–2%, Karki et al. 1997).

Geodynamic interpretations

Avants et al. (2006); Lay et al. (2006) and Ohta et al. (2008) have investigated the detailed S-wave structure of the D″-region within the northeastern part of the Pacific LLSVP. Figures 9 and 10 are redrawn from Ohta et al. (2008). These investigators developed S-wave models with four discontinuities in the lowermost 250–450 km above the CMB, with arrivals between the direct S-wave and the core-reflected ScS-wave arrivals (Fig. 10). Whereas the lowermost discontinuity represents the transition to the ultra-low velocity zone (ULVZ), there are some uncertainties associated with the upper three discontinuities.

Lay et al. (2006) focussed on the large lateral variation in depth to the discontinuities and proposed rapid thinning of a thermochemical pile from 450 km to 230 km over a distance of 3° towards NE, accompanied by lateral flow of hot material within the lower portion of the pile towards the NE margin. They interpreted the uppermost discontinuity characterized by an S-velocity decrease as the top of the thermo-chemical pile and the two middle discontinuities as the top and bottom of a ppv-rich lens within the pile. The interpreted ppv-lens is also thinning towards NE from 255 km to 60 km over 3°. The ULVZ-layer was observed to thicken from 10-15 km to 50 km in the same direction. A schematic and interpretative illustration of these features is shown in Fig. 11a.

Added seismological data and a partial reinterpretation of the Lay et al. model were presented by Ohta et al. (2008)

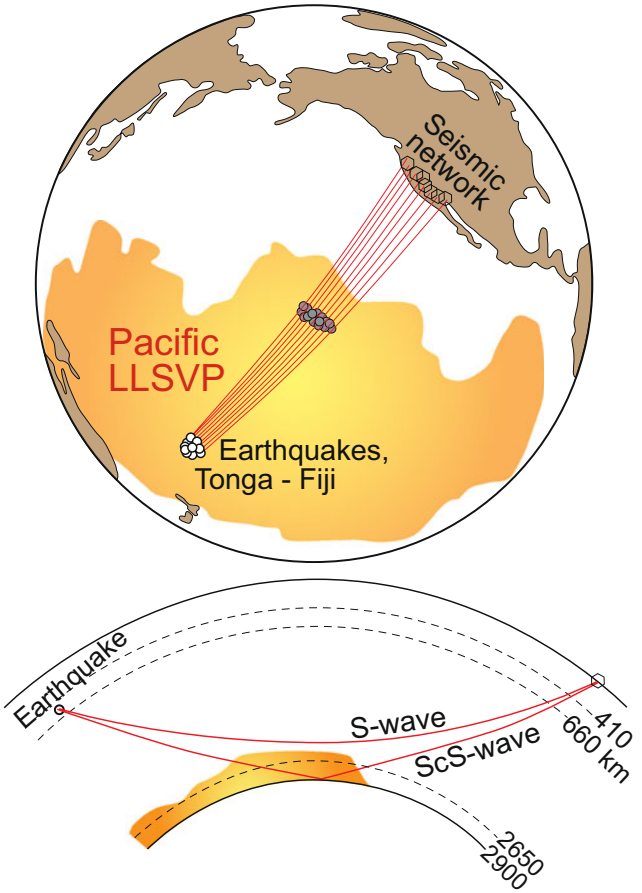

Fig. 9 Schematic illustration of the Pacific LLSVP and the source and receiver geometry used in the S-wave mapping studies by Avants et al. (2006); Lay et al. (2006) and Ohta et al. (2008)

(Fig. 11b). The reinterpretation is based on their experimental data (Fig. 7) and the indication that the coincident pv-ppv- and silica-rich phase transitions in basaltic material in combination may cause S-velocity decrease. This is in

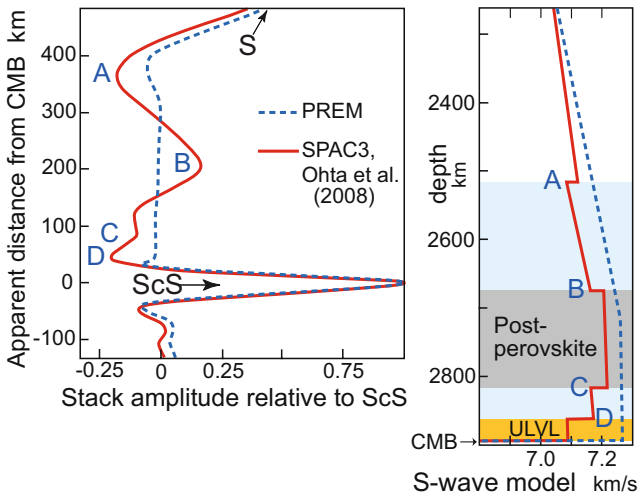

Fig. 10 S-wave model of Ohta et al. (2008)

contrast to the expected and observed S-velocity increase of the pv-ppv-transition in peridotitic material. The thermo-chemical pile material is most likely a mechanical mixture of basaltic and peridotitic lithologies with a higher basalt/peridotite ratio than the avarage mantle. The very low diffusivity of the major lower mantle mineral perovskite (Holzapfel et al. 2005) requires homogenization of heterogeneities to occur by unrealistically intense mechanical

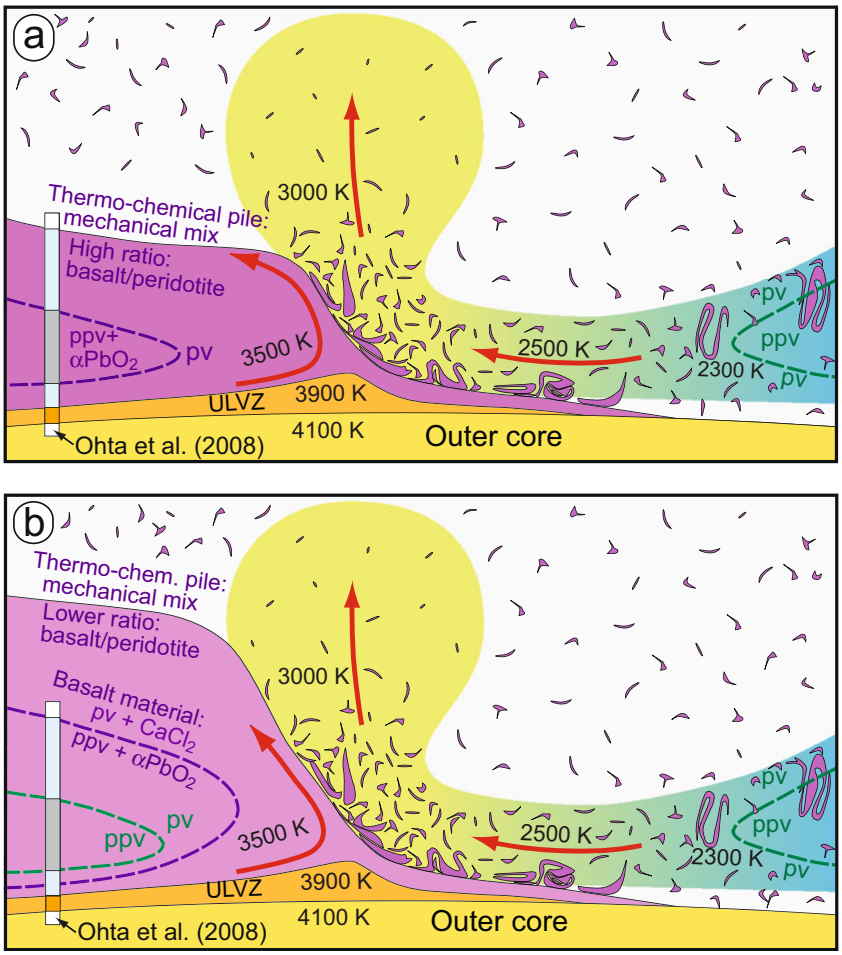

Fig. 11 Schematic illustration of a plume generation zone at the steep margin of a thermochemical pile (LLSVP). The figure, largely based on Lay et al. (2006), shows the thermal and physical interaction between cold material from mantle downwelling areas and hot material within the thermochemical pile. Lateral flow (right to middle) of cool recycled oceanic lithosphere with deformed layers and patches of basaltic crust (dark) undergoes gradual T-increase (approximate temperatures in K) by heating near the CMB. The folded and disrupted slivers of basaltic material within the relatively cool mantle flow are assumed to be in the ppv-field. The stippled lines mark the approximate pv-ppv boundaries in peridotitic and basaltic materials, respectively. Density-based separation of basaltic and peridotitic lithologies may be facilitated by basaltic assemblages undergoing the ppv-transition and the silica phase transition ($CaCl_2$- to αPbO_2-structure) at lower p for a given T compared to peridotitic lithologies and by the higher intrinsic (chemical) density of basaltic lithologies. The two panels (A and B) represent alternative interpretations of the seismo-stratigragraphic column of Ohta et al. (2008). The indicated column (S-wave model from Fig. 8) is identical in panels A and B. Panel A reflects the original interpretation of Lay et al. (2006), where the uppermost, S-wave-drop-discontinuity (Fig. 8) is the top of the thermochemical pile. The two next discontinuities are the double-crossing of the reaction from pv (+$CaCl_2$) to ppv (+αPbO_2) in basaltic material. The interpretation of the lowermost discontinuity above the CMB as the ultra-low velocity zone (ULVZ) is identical for the two panels. Panel B is consistent with the new interpretation of Ohta et al. (2008), who emphasize that the thermochemical piles are probably mechanical mixtures of peridotite and basalt, because thermal diffusion in the lower mantle is very slow (e.g. Holzapfel et al. 2005). In panel B the thermochemical pile is thicker (thickness is chosen arbitrarily), and volume ratio basalt/peridotite is assumed to be lower than in panel A. The uppermost discontinuity is re-interpreted by Ohta et al. (2008) to be the reaction from pv (+$CaCl_2$) to ppv (+αPbO_2) in basaltic material. In basaltic material with high Fe/Mg-ratio and high Al-content, the shear velocity may drop at the pv-ppv-transition (Caracas and Cohen 2005; Tsuchiya and Tsuchiya 2006). The two middle discontinuities (increasing and decreasing S-velocities at the upper and lower disc., respectively) are interpreted to be the pv- to ppv- and the ppv- to pv-transitions, respectively, in peridotitic material. The border areas of the thermochemical piles would be efficient sites for the generation of large, episodic mantle plumes. The concave interface along the intersection of the sub-horizontal thermal boundary layer (TBL, hot-plate) of the CMB and a steep TBL along the pile margin represents a favourable location for the initiation of thermal buoyancy. This will also be the most favourable location for the physical separation of dense basaltic patches and slivers from the lighter peridotite (see text)

mixing and shearing. If the proportions of basaltic and peridotitic lithologies within the thermochemical piles are approximately sub-equal (e.g. in the 30–70% range), it may be possible to observe the phase transitions within both of the separate lithologies seismically. Ohta et al. (2008) ascribe the uppermost discontinuity (A in Fig.10) to the combined pv-ppv and silica ($CaCl_2$ to α-PbO_2) phase transitions in basaltic material and the two intermediate discontinuities (B and C in Fig. 10) to the pv-ppv-trasition in peridotite lithologies (double-crossing of the transition, Hernlund et al. 2005). Based on the phase relations and the vertical distance between the discontinuities they suggest that the temperature at the uppermost basaltic discontinuity (A) is 400–500 K lower that of the uppermost peridotitic discontinuity (B). The vertical distance between the uppermost and the two intermediate discontinuities will be a reflection of the relative displacement of the phase boundaries for basaltic and peridotitic lithologies, their overall Clapeyron slopes and the vertical thermal gradient across the D″ region.

Figure 11 illustrates the likely mechanism of partial density separation of basaltic and peridotitic material and the possible accretion of basaltic material to the margin of the thermochemical piles. The lateral flow of cold mantle with large proportions of subducted lithosphere (from the right hand side) along the CMB will lead to gradual heating of this composite material. The lateral flow is deflected by the relatively steep margin of a thermochemical pile. Heating continues along the hot and concave margin interface, developing thermal buoyancy, especially of low-density peridotite material. Therefore, this is a favourable location for density-driven separation of basaltic patches and slivers from a developing plume enriched in the peridotite matrix component. Such a model is consistent with the inferences of Sobolev et al. (2007) that mantle plumes generally have a limited capability of entraining and carrying basaltic material.

The nature of chemical re-equilibration between core and mantle

Reactions between outer core metal and the silicates and oxides of the lowermost mantle have been suspected, and several studies have found tentative evidence for such interaction (e.g. Knittle and Jeanloz 1989, 1991; Brandon et al. 1998). Other studies, however, have rejected the proposed contamination of the mantle with core metal (Schersten et al. 2004; Luguet et al. 2008). Because most of the planetary accretion occurred at considerably lower oxygen fugacities than those of the present planetary mantles and the early core segregation also occurred under such low fO_2, the present mantle may well be undersaturated with respect to oxygen or FeO. There is mounting evidence for the extraction to the core of the FeO and SiO_2-components of pv and fp of the lowermost mantle (Takafuji et al. 2005; Asahara et al. 2007; Ozawa et al. 2008). The X_{MgSiO3} and X_{MgO} of pv and fp in equilibrium with the Earth's core at about 135 GPa and 3500–4000 K may be as high as 0.999 and 0.97, respectively. The extremely low cation diffusion rate of pv (Holzapfel et al. 2005) may limit the extent of the FeO-depleted zone to a few metres of the lowermost mantle. Therefore, the potential density instability resulting from the extraction of the FeO-component from pv and fp into the core may be so small that a thin lowermost FeO-depleted mantle layer simply remains in place as a seal, preventing further extensive mantle-core reaction.

Spin transition of Fe and radiative thermal conductivity in the D″-zone

The Fe/Mg-partitioning between the lower mantle minerals will be significantly affected by possible spin transitions of ferrous and/or ferric iron (e.g. Badro et al. 2003, 2004; Lin et al. 2007a). The early studies by Badro et al. (2003, 2004) of the Fe-spin state in ferropericlase and perovskite by synchrotron-based X-ray emission spectroscopy were carried out at high-pressure, but room temperature. They observed a high- to low-spin transition in fp at 60–70 GPa and two electronic transitions at 70 GPa (high- to intermediate spin) and 120 GPa (intermediate- to low-spin) for pv. As pointed out by Hofmeister (2006), low- to high-spin transitions have generally positive dp/dT-slopes and may therefore not occur at mantle temperatures. The recent high-temperature studies by Lin et al. (2008) and McCammon et al. (2008) indicate that Fe^{2+} in pv transforms to an intermediate spin state in the upper part (about 30 GPa) of the lower mantle and remains like this throughout the rest of the lower mantle. An intermediate spin state appears to occur also in ppv. The ferrous iron in fp, however, transforms from high- via intermediate- to the low-spin at pressures of 35–90 GPa (Lin et al. 2007b). The indications of change to intermediate spin in pv at 800–1000 km depth, followed by gradual spin transitions in fp at depths of 900–2200 km, agree with the apparent lack of seismic discontinuities or distinct transition zones in the intermediate parts of the lower mantle.

The spin states of Fe^{2+} and Fe^{3+} in minerals like pv and fp can also potentially influence the radiative thermal conductivity. Plume generation and convective vigour within the large thermal gradients of the D″-zone will depend on the magnitude of the thermal conductivity under these conditions. The radiative conductivity is highest within the infrared range at lowermost mantle temperatures of 2500–3500 K (e.g. Li 2007). In minerals with high-spin iron the radiative conductivity is hindered by absorption in the near-infrared spectral region due to intraband transitions

(Badro et al. 2004). A transition to low-spin iron will shift these absorption bands to the visible (green-blue) region. In their laser-heating experiments with Fe-bearing perovskite, Badro et al. (2004) found that heating with the IR-laser was no longer possible at 120 GPa and interpreted this to increased IR-transparency caused by a low-spin transition. Because pv and ppv both appear to be in an intermediate spin state throughout the lower 2000 km of the mantle, the associated radiative conductivity effects are not expected to be large.

Recently, the IR to UV absorption spectra have been measured for pv and fp up to 125–133 GPa at room temperature. Keppler et al. (2008) recorded low optical absorption at the highest pressures and estimate the radiative contribution of the thermal conductivity of the lowermost mantle to be about 10 Wm^{-1} K^{-1}, whereas Goncharov et al. (2008) suggests drastically lower thermal conductivities, with a radiative contribution of less than 0.54 Wm^{-1} K^{-1}.

Based on the pT-location and Clapeyron slope of the pv-ppv-transition boundary, the absolute temperatures and temperature gradients across the D″-zone can be estimated where seismological data on the depth to the D″-discontinuities are available. By assuming a value (e.g. 10 Wm^{-1} K^{-1}) for the thermal conductivity, the heat flux through the D″-zone can also be derived. Van der Hilst et al. (2007) and Lay et al. (2008) derive estimates for the total CMB-heat flow of 7–15 TW, based on a dp/dT-slope of the pv-ppv-transition of 7–10 MPa/K and the observed D″-discontinuities under the Caribean and central-NE Pacific. Such high values may require a significant additional radioactive heat source in the outer core, e.g. potassium. From a geochemical point of view, it seems unlikely that radioactive heat from K in the core would contribute much more than about 0.2 TW (Corgne et al. 2007).

As pointed out by Tateno et al. (2009), a Clapeyron slope of about 13 MPa/K would be more consistent with a lower CMB-temperature of about 3700 K and a global heat flux of 6–7 TW from the core. For a given mantle adiabat (e.g, Ono 2008) and seismologically observed depths of the double crossings of the pv-ppv-transition in an "average" mantle, Fig. 12a shows schematically the effects of changing the dp/dT-slope of the phase boundary from 8 to 13 MPa/K. The uncertainties regarding the thermal conductivity of the lowermost mantle (e.g. Goncharov et al. 2008; Keppler et al. 2008) may potentially change this situation. A particular CMB-temperature for a given ppv-layer may be consistent with either high radiative and total thermal conductivity in combination with a large dp/dT-slope or lower conductivity combinied with a lower dp/dT-slope (Fig. 12b). Therefore, the relatively high dp/dT-slope of the pv-ppv transition indicated by the experimental study of $MgSiO_3$ by Tateno et al. (2009) may also be consistent with high thermal conductivity and high CMB-temperature.

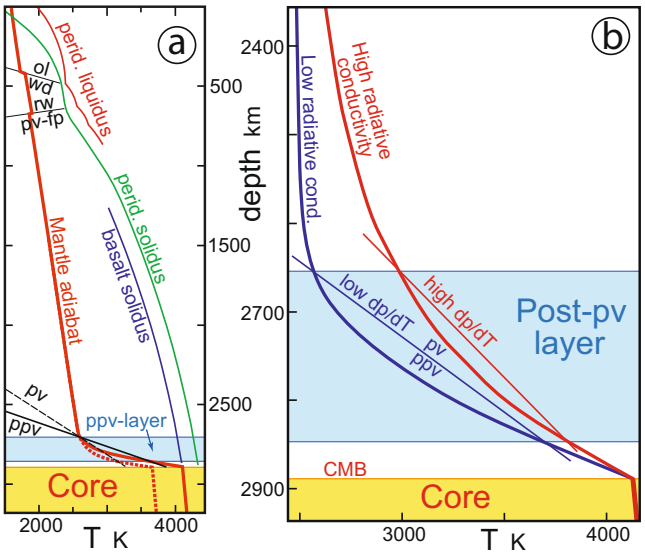

Fig. 12 Mantle adiabat and local geothermal gradients in the D″-zone compared to different dp/dT-slopes and locations of the pv-ppv-phase boundary. Left panel (**a**): The mantle adiabat is from Ono (2008) and Stixrude et al. (2009). The basalt solidus is from Hirose et al. (1999) and the peridotite liquidus and solidus are compiled from Zhang and Herzberg (1994); Herzberg et al. (2000), Trønnes and Frost (2002); Ito et al. (2004) and Zerr et al. (1998). The solid pv-ppv phase boundary for a pyrolite composition is from Ono and Oganov (2005) and has a dp/dT-slope of 8 MPa/K. The stippled pv-ppv-boundary has a larger dp/dT-slope of about 13 MPa (Tateno et al. 2009). A larger slope of 13 MPa/K could indicate that the CMB-temperature is 300–500 K lower than for an 8 MPa/K-slope (stippled geothermal gradient). An alternative possibility is shown in the right panel (**b**). In this model the CMB-temperature is the same for two different geothermal gradients, representing different thermal conductivity in the lowermost mantle. A pv-ppv-transition with a high dp/dT-slope under conditions of high thermal conductivity results in the same ppv-layer as a transition boundary with a lower Clapeyron slope and associated with lower thermal conductivity. This particular model also assumes that the transition temperature at a given depth is slightly higher for the high dp/dT-slope scenario

Geochemical evidence for the existence of isolated mantle reservoirs

The need for one or more mantle reservoirs that have remained completely or partially isolated from the convecting mantle or upper mantle over most of Earth's history has been pointed out by several workers (e.g. Jacobsen and Wasserburg 1979; O'Nions et al. 1979; Kellogg et al 1999; Tolstikhin and Hofmann 2005; Boyet and Carlson 2005). The early concept of a distinct layering at the 660 km discontinuity (with MORB sampling the upper depleted mantle and oceanic island basalts sampling also a primordial lower mantle) was rejected by seismic tomographic results showing clear signs of subducted slab penetration into the lower mantle. Based on chondritic models for the Earth and for the mantle, the geochemical inventory of the entire convecting mantle that is intermittently sampled by a range of volcanic products (basalts, kimberlites, carbona-

tites) emplaced at the Earth's surface seems to be depleted in several of the lithophile incompatible elements, including the heat producing elements. With their "lava lamp" model, Kellogg et al. (1999) and van der Hilst and Karason (1999) suggested that the lowermost 1300 km of the mantle was enriched in these elements and had a sufficient intrinsic density to resist entrainment into the general mantle convection. The depth to the upper boundary of this lower enriched part of the mantle was thought to vary temporally between different regions, in accordance with current seismic tomography images. Substantial support for this model did not materialize, and the LLSVPs and ULVZs within the D″ region are now considered better candidates for partly or completely isolated geochemical reservoirs.

Recent analysis of a range of mantle derived products in terms of the short-lived ^{146}Sm-^{142}Nd system (half-life of 103 Ma) indicate the presence of mostly isolated and unsampled enriched reservoir(s) formed within the first 400–500 Ma of Earth history (Boyet and Carlson 2005, 2006; Upadhyay et al. 2009). The ULVZ- or LLSVP-material could possibly represent such KREEP-like reservoirs. The large majority of mantle-derived magmatic rocks (komatiites, basalts, kimberlites and carbonatites) have uniform ^{142}Nd/^{144}Nd-ratios mostly within the range of the current analytical uncertainty, but significantly higher than those in ordinary chondrites. Therefore, if the Sm/Nd-ratio of bulk silicate Earth is approximately chondritic, the sampled convective mantle must have undergone very early melt depletion and be geochemically balanced by enriched material. As mentioned above, the overall melt-depleted character of the convecting mantle is supported by a range of other geochemical data.

A few exceptions to the uniform ^{142}Nd/^{144}Nd-ratios of ordinary mantle-derived rocks include elevated ratios in 4.3 Ga old crust of the Nuvvuagittuq greenstone belt of northern Quebec (O'Neil et al. 2008) and lower ratios in 3.9–3.6 Ga crust of Isua, Greenland (Boyet and Carlson 2006) and in 1.5 Ga alkaline rocks derived from the lithospheric root of the Bastar craton in eastern India (Upadhyay et al. 2009). Even if Earth, Moon and Mars may have slightly supra-chondritic Sm/Nd-ratios, as suggested by Caro et al. (2008), the overall refractory nature of the convecting mantle seems to require enriched reservoir(s) with ^{142}Nd/^{144}Nd-ratios considerably lower than those measured in the Bastar and the Nuvvuagittuq rocks (Upadhyay et al. 2009).

Although the origin and material properties of the two large thermochemical piles are still uncertain, density-driven separation and accumulation of mantle material with a high basalt/peridotite ratio may be the most likely mechanism (Fig. 11). In this scenario the piles may have grown gradually during much of the Earth's history. However, other proposed scenarios for the development of chemically distinct (generally melt enriched) reservoirs near the CMB are linked to processes operating during early Earth differentiation or during the first 100–500 Ma. Several computational and experimental studies have indicated that silicate melt may be denser than the coexisting solid residue in the lowermost mantle (e.g. Stixrude and Karki 2005; Mosenfelder et al. 2007; Stixrude et al. 2009). These results led Labrosse et al. (2007) to suggest a separate lower mantle magma ocean crystallizing pv and fp in the uppermost part. With progressive crystallization, the residual melt would become Fe-enriched and the later Fe-rich cumulates would be dense enough to avoid entrainment in rising convective flow. According to this model, the thermochemical piles could be accumulations of such dense cumulates and the ULVZ-material next to the CMB could be partially molten (mushy) residual magma ocean material.

Another partly related scenario for the origin of thermochemical piles in the D″ region is that they may be formed by sinking and accumulation of dense lithologies involving a considerable proportion of solidified melt veins formed in the lower part of the upper mantle (Lee et al. 2008). During the early Earth history the temperatures in hot plumes may have exceeded the solidus at pressures greater than 9 GPa (depths below 300 km) in the upper mantle. At these conditions the melt will be denser than the coexisting olivine-dominated solid residue. The melts formed at such depths might percolate downwards and then freeze again as they cross their pressure-dependent solidi. Beneath areas of extensive and repeated plume-melting activity below 300 km depths, the local volume proportion of dense solidified vein material may be sufficient to cause gravitational instabilities that could lead to minor avalanches through the lower mantle and accumulations of proto-piles resting on the CMB.

A third scenario for the accumulation of melt-enriched material in the lowermost mantle was proposed by Tolstikhin and Hofmann (2005) and Tolstikhin et al. (2006). Their model involves the subduction of the earliest oceanic crust (4.5–3.9 Ga), containing a significant impact-generated accumulation of chondritic and rather Fe-rich meteoritic material. Either of these models may represent a solution for the geochemical discrepancy between probable bulk Earth and bulk mantle models and the inferred composition of the "accessible" convecting mantle sampled by basalts, kimberlites and carbonatites emplaced on or near the Earth's surface.

Concluding remarks

Our general insights into the structure and dynamics of the lowermost mantle has improved considerably since the

2004-discovery of the pv-ppv transition. In spite of many remaining uncertainties, not the least in terms of the phase relations, mineral physics and geochemistry, the pictures that emerge from seismological observations, the paleomagnetic/paleogeographic relocation of LIP-sites and geodynamic modelling provide important guidelines. The indications of long-term (>300 Ma) preservation of the presently observed Pacific and African thermochemical piles (LLSVPs) puts important constraints on the excess density of these regions. The Pacific and African geoid highs may largely reflect the excessive density of these piles, and the inferred long-term stability has important implications for the evolution of the geochemically accessible convecting mantle. Although complete information concerning the regional depth variation of the D″-discontinuities and the regional distribution of ultra-low velocity zones and seismic anisotropy is lacking, the preliminary indications seem to support a general mantle flow pattern illustrated in Fig. 13. Mantle convection is mostly driven by the sinking of cold and dense lithosphere, coupled with a very slow and relatively pervasive counterflow, interspersed with spatially and temporally limited plumes of variable sizes (e.g. Davies 1998; van Keken et al. 2002; Bercovici 2003). A major portion of the slow counterflow is likely confined to the regions above the LLSVPs. The proportion of heat transported by plumes (plume flux) relative to total upwards heat flow has been calculated by several workers. Estimates of 10–15% (e.g. Davis 1998) would correspond to common estimates of core heat flux. However, Malamud and Turcotte (1999) suggested an order of magnitude higher plume flux, invoking a very large

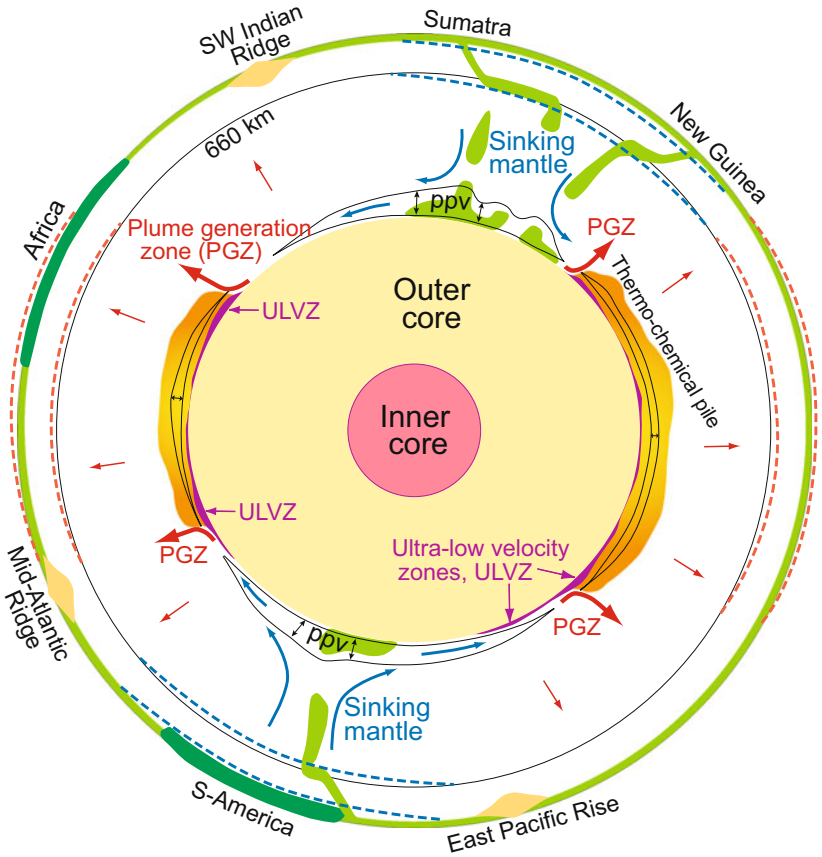

Fig. 13 Schematic equatorial Earth section. The thick stippled lines mark areas with geoid lows and highs. The geoid highs may largely reflect the excessive density of the underlying thermochemical piles. The 660 km discontinuity and stipulated stability range of ppv are indicated by thin lines. For a given pressure (depth), the ppv stability field is likely to expand with (1) decreasing temperature and (2) increasing Fe/Mg ratio (or basalt/peridotite ratio). The ppv-stability range is therefore significant within the hot and dense piles enriched in recycled basaltic crustal material. The margins of the Pacific and African thermochemical piles (LLSVPs) are favourable locations for the episodic initiation of large mantle plumes. The main mantle circulation is shown by sinking regions of Mesozoic to present subduction, probably coupled with a slow and pervasive counterflow of ascending low-density mantle above the dense and hot LLSVPs. The ascending low-density mantle is comparatively hot and may have a slightly reduced basalt/peridotite mass ratio due to the preferential extraction of basaltic material to the thermochemical piles. The figure is not drawn exactly to scale and the thickness of the ULVZs, in particular, is exaggerated in order to render these features visible

number of small plumes (about 5200) that might otherwise be considered part of a slow and pervasive flow. They further suggested that the large number of Pacific seamounts may be the expression of such small plumes.

From a global geodynamic point of view, the mass and density distribution of the Earth must be in balance with the rotation axis. The dense thermochemical piles with overlying hot and rising mantle and the cold mantle regions with downwelling associated with Mesozoic to recent subduction zones are directly reflected by the geoid shape and are geometrically linked to the rotation axis (e.g. Richards et al. 1997; Steinberger and Torsvik 2008). Compared to the mantle, the core has a nearly homogenous density distribution and spherical shape.

The indication that the great majority of more than 20 large igneous provinces erupted throughout the last 300 Ma originated from episodic plume generation at the margins of the thermochemical piles has important implications for the dynamics of the CMB-region and Earth's evolution. The mechanism for initiation of these plumes and the factors that may determine their spatial distribution and the interval between them is uncertain. Intermittent mantle avalanches of partially accumulated oceanic lithosphere from the transition zone may trigger plume generation at the CMB. The endothermic perovskite-forming reaction responsible for the 660 km discontinuity has been suspected to modulate mantle flow in space and time.

Further progress in our understanding of the structure, mineralogy and dynamics of the lowermost mantle will undoubtedly result from the combined effort in seismological mapping, geodynamic modelling and the determination of experimental phase relations and physical properties of candidate materials. Some of the main high-pressure experimental challenges include the establishment of a consistent and accurate pressure scale and the development of more reliable laser heating aiming at reduced thermal gradients near the laser hot-spot. The development of improved multianvil technology with sintered diamond cubes can potentially also reach the pT-condition of the D″-zone. Ab inito DFT-modelling will remain a powerful and independent complement to high-pT experimentation. Further development of this technique to deal with more complex chemical compositions and partially disordered systems will represent an important improvement.

Acknowledgements I appreciate editorial encouragement from Jürgen Konzett, a perceptive review from Kevin Burke and helpful corrections from an anonymous reviewer and Maarten Aerts. The Nansen Foundation of the Norwegian Academy of Science and Letters, the Bayerisches Geoinstitut under the EU Programme "Research Infrastructures: Transnational Access" (Contract No. 505320, RITA, High Pressure) and NHM, University of Oslo provided financial and institutional support.

References

Akber-Knutson S, Steinle-Neumann G, Asimow PD (2005) Effect of Al on the sharpness of the $MgSiO_3$ perovskite to postperovskite phase transition. Geophys Res Lett 32:L14303

Andrault D, Bolfan-Casanova N (2001) High-pressure phase transformations in the $MgFe_2O_4$ and Fe_2O_3-$MgSiO_3$ systems. Phys Chem Mineral 28:211–217

Anderson DL (1982) Hotspots, polar wander, Mesozoic convection and the geoid. Nature 297:391–393

Asahara Y, Frost DJ, Rubie DC (2007) Partitioning of FeO between magnesiowustite and liquid iron at high pressures and temperatures: implications for the composition of the Earth's outer core. Earth Planet Sci Lett 257:435–449

Auzende A-L, Badro J, Ryerson FJ, Weber PK, Fallon SJ, Addad A, Siebert J, Fiquet G (2008) Element partitioning between magnesium silicate perovskite and ferropericlase: new insights into bulk lower-mantle geochemistry. Earth Planet Sci Lett 269:164–174

Avants M, Lay T, Russell SA, Garnero EJ (2006) Shear-velocity variation within the D″ region beneath the Central Pacific. J Geophys Res 111:B05305. doi:10.1029/2004JB003270

Badro J, Fiquet G, Guyot G, Rueff J-P, Stuzhkin VV, Vanko G, Monaco G (2003) Iron partitioning in Earth's mantle: toward a deep lower mantle discontinuity. Science 300:383–386

Badro J, Rueff J-P, Vanko G, Monaco G, Fiquet G, Guyot G (2004) Electronic transitions in perovskite: possible nonconvecting layers in the lower mantle. Science 305:789–791

Becker TW, Boschi L (2002) A comparison of tomographic and geodynamic mantle models. Geochem Geophys Geosys 3:2001GC000168

Bercovici D (2003) The generation of plate tectonics from mantle convection. Earth Planet Sci Lett 205:107–121

Boffa-Ballaran T, Trønnes RG, Frost DJ (2007) Equations of state of $CaIrO_3$ perovskite and post-perovskite phases. Am Mineral 92:1760–1763

Boyet M, Carlson RW (2005) ^{142}Nd evidence for early (4.53 Ga) global differentiation of the silicate Earth. Science 309:576–581

Boyet M, Carlson RW (2006) A new geochemical model for the Earth's mantle inferred from ^{146}Sm—^{142}Nd systematics. Earth Planet Sci Lett 250:254–268

Brandon AD, Walker RJ, Morgan JW, Norman MD, Prichard HM (1998) Coupled ^{186}Os and ^{187}Os evidence for core-mantle interaction. Science 280:1570–1573

Bullen KE (1949) Compressibility-pressure hypothesis and the Earth's interior. Mon Not R Astr Soc 5:355–368

Burke K, Torsvik TH (2004) Derivation of large igneous provinces of the past 200 million years from long-term heterogeneities in the deep mantle. Earth Planet Sci Lett 227:531–538

Burke K, Steinberger B, Torsvik TH, Smethurst MA (2008) Plume Generation Zones at the margins of large low shear velocity provinces on the core-mantle boundary. Earth Planet Sci Lett 265:49–60

Caracas R, Cohen RE (2005) Effect of chemistry on the stability and elasticity of the perovskite and postperovskite phases in the $MgSiO_3$-$FeSiO_3$-Al_2O_3 system and implications for the lowermost mantle. Geophys Res Lett 32:L16310

Caro G, Bourdon B, Halliday AN, Quitte G (2008) Super-chondritic Sm/Nd ratios in Mars, the Earth and the Moon. Nature 452:336–339

Corgne A, Keshav S, Fei Y, McDonough WF (2007) How much potassium is in the Earth's core? New insights from partitioning experiments. Earth Planet Sci Lett 256:567–576

Davaille A, Girard F, Le Bars M (2002) How to anchor hotspots in a convecting mantle? Earth Planet Sci Lett 203:621–634

Davaille A, Stutzmann E, Silveira G, Besse J, Courtillot V (2005) Convective patterns under the Indo-Atlantic box. Earth Planet Sci Lett 239:233–252

Davies GF (1998) Plates, plumes, mantle convection and mantle evolution. In: Jackson I (ed) The Earth's mantle. Composition, structure and evolution. Cambridge Univ Press, 228-258

Dobson DP, Brodholt JP (2005) Subducted banded iron formations as a source of ultralow-velocity zones at the core-mantle boundary. Nature 434:371–374

Dziewonski AM, Anderson DL (1984) Seismic tomography of the Earth's interior. Am Scientist 72:483–494

Forte AM, Mitrovica JX (2001) Deep-mantle high viscosity flow and thermochemical structure inferred from seismic and geodynamic data. Nature 410:1049–1056

Frost DJ (2003) The structure and sharpness of (Mg, Fe)2SiO4 phase transformations in the transition zone. Earth Planet Sci Lett 216:313–328

Frost DJ, Liebske C, Langenhorst F, McCammon CA, Trennes RG, Rubie DC (2004) Experimental evidence for the existence of iron-rich metal in the Earth's lower mantle. Nature 428:409–412

Garnero EJ, McNamara AK (2008) Structure and dynamics of Earth's lower mantle. Science 230:626–628

Garnero EJ, Lay T, McNamara AK (2007) Implications of lower-mantled structural heterogeneity for the existence and nature of whole-mantled plumes. In: Foulger GR, Jurdy DM (eds) The origin of melting anomalies: plates, plumes and planetary processes. Geol Soc Am Spec Pap 430:79–102

Goncharov AF, Haugen BD, Struzhkin VV, Beck P, Jacobsen SD (2008) Radiative conductivity in the Earth's lower mantle. Nature 456:231–234

Guignot N, Andrault D, Morard G, Bolfan-Casanova N, Mezouar M (2007) Thermodynamic properties of post-perovskite phase $MgSiO_3$ determined experimentally at core-mantled boundary P-T conditions. Earth Planet Sci Lett 256:162–168

Helffrich GR, Wood BJ (1996) 410 km discontinuity sharpness and the form of the olivine phase diagram: resolution of apparent seismic contradictions. Geophys J Int 126:7–12

Hernlund JW, Thomas C, Tackley PJ (2005) A doubling of the post-perovskite phase boundary and structure of the Earth's lowermost mantle. Nature 434:882–886

Herzberg C, Raterron P, Zhang J (2000) New experimental observations on the anhydrous solidus for peridotite KLB-1. Geochem Geophys Geosyst 1:2000GC000089

Hirose K (2006) Postperovskite phase transition and its geophysical implications. Rev Geophys 44:RG3001

Hirose K, Fei Y, Ma Y, Mao H-K (1999) The fate of subducted basaltic crust in the Earth's lower mantle. Nature 397:53–56

Hirose K, Takafuji N, Sata N, Ohishi Y (2005) Phase transition and density of subducted MORB crust in the lower mantle. Earth Planet Sci Lett 237:239–251

Hofmeister AM (2006) Is low-spin Fe^{2+} present in Earth's mantle? Earth Planet Sci Lett 243:44–52

Holzapfel C, Rubie DC, Frost DJ, Langenhorst F (2005) Fe-Mg interdiffusion in (Mg,Fe)SiO_3 perovskite and lower mantle reequilibration. Science 309:1707–1710

Hutko AR, Lay T, Garnero EJ, Revenaugh J (2006) Seismic detection of folded, subducted lithosphere at the core-mantle boundary. Nature 441:333–336

Iitaka T, Hirose K, Kawamura K, Murakami M (2004) The elasticity of the $MgSiO_3$ post-perovskite phase in the Earth's lowermost mantle. Nature 430:442–445

Irifune T, Tsuchiya T (2007) Mineralogy of the Earth — Phase transitions and mineralogy of the lower mantle. In: Price GD and Schubert G (eds) Treatise on Geophysics, Vol 2 Mineral Physics, 33–62

Ito E, Kubo A, Katsura T, Walter MJ (2004) Melting experiments of mantle materials under lower mantle conditions with implications for magma ocean differentiation. Phys Earth Planet Int 143–144:397–406

Jacobsen SB, Wasserburg GJ (1979) The mean age of mantle and crustal reservoirs. J Geophys Res 84:7411–7427

Karki BB, Stixrude L, Crain J (1997) Ab initio elasticity of the three high-pressure polymorphs of silica. Geophys Res Lett 24:3269–3272

Kellogg LH, Hager BH, van der Hilst RD (1999) Compositional stratification in the deep mantle. Science 283:1881–1884

Keppler H, Dubrovinsky LS, Narygina O, Kantor I (2008) Optical absorption and radiative thermal conductivity of silicate perovskite to 125 gigapascals. Science 322:1529–1532

Kesson SE, Fitz Gerald JD, Shelley JM (1998) Mineralogy and dynamics of a pyrolite lower mantle. Nature 393:252–255

Knittle E, Jeanloz R (1989) Simulating the core-mantle boundary: an experimental study of high-pressure reactions between silicates and liquid iron. Geophys Res Lett 16:609–612

Knittle E, Jeanloz R (1991) Earth's core-mantle boundary: results of experiments at high pressures and temperatures. Science 251:1438–1443

Kobayashi Y, Kondo T, Ohtani E, Hirao N, Miyajima N, Yagi T, Nagase T, Kikegawa T (2005) Fe-Mg partitioning between (Mg, Fe)SiO_3 postperovskite, perovskite, and magnesiowustite in the Earth's lower mantle. Geophys Res Lett 32:L19301

Labrosse S, Hernlund JW, Coltice N (2007) A crystallizing dense magma ocean at the base of the Earth's mantle. Nature 450:866–869

Lay T (2005) The deep mantle thermo-chemical boundary layer: the putative mantle plume source. In: Foulger GR, Natland JH, Presnall DC, Anderson DL (eds) Plates, plumes and paradigms. Geol Soc Am Spec Pap 388:193–205

Lay T, Helmberger DV (1983) A lower mantle S-wave triplication and the shear velocity structure of D″. Geophys J R Astron Soc 75:799–838

Lay T, Williams Q, Garnero EJ (1998) The core-mantle boundary layer and deep Earth dynamics. Nature 392:461–468

Lay T, Garnero EJ, Williams Q (2004) Partial melting in a thermo-chemical boundary layer at the base of the mantle. Phys Earth Planet Int 146:441–467

Lay T, Hernlund J, Garnero E, Thorne MS (2006) A post-perovskite lens and D″ heath flux beneath the central Pacific. Science 314:1272–1276

Lay T, Hernlund J, Buffett BA (2008) Core-mantle boundary heat flow. Nature Geosci 1:25–32

Lee C, Luffi P, Plank T, Dalton H, Leeman W, Hoink T, Li J, Masters G (2008) Secular changes in the style of mantle melting and mantle differentiation as constrained by the depths and temperatures of magma genesis. Eos Trans Am Geophys Union 89(53) Fall Meet Suppl Abstr DI34A-03

Li J (2007) Electronic transitions and spin states in the lower mantle. In: Hirose K, Brodholt J, Lay T, Yuen D (eds) Post-perovskite. The last mantle phase transition. Am Geophys Union Geophys Monogr 174:47–68

Lin JF, Jacobsen SD, Wentzcovitch RM (2007a) Electronic spin transition of iron in the Earth's deep mantle. Eos Trans Am Geophys Union 88:13–17

Lin JF, Vanko G, Jacobsen SD, Iota V, Struzhkin VV, Prapenka VB, Kuznetsov A, Yoo C-S (2007b) Spin transition zone in Earth's lower mantle. Science 317:1740–1743

Lin J-F, Watson H, Vanko G, Alp EE, Prakapenka VB, Dera P, Stuzhkin VV, Kubo A, Zhao J, McCammon C, Evans WJ (2008) Intermediate-spin ferrous iron in lowermost mantle post-perovskite and perovskite. Nature Geosci 1:688–691

Luguet A, Pearson DG, Nowell GM, Dreher ST, Coggon JA, Spetsius ZV, Parman SW (2008) Enriched Pt-Re-Os isotope systematics in plume lavas explained by metasomatic sulfides. Science 319:453–456

Lundin S, Catalli K, Santillan J, Shim SH, Prakapenka VB, Kunz M, Meng Y (2008) Effect of Fe on the equation of state of mantle silicate perovskite over 1 Mbar. Phys Earth Planet Int 168:97–102

Malamud BD, Turcotte DL (1999) How many plumes are there? Earth Planet Sci Lett 174:113–124

Mao WL, Shen G, Prakapenka VB, Meng Y, Cambell AJ, Heinz D, Shu J, Hemley RJ, Mao HK (2004) Ferromagnesian postperovskite silicates in the D″ layer of the Earth. Proc Natl Acad Sci USA 101:15867–15869

Mao WL, Meng Y, Shen G, Prakapenka VB, Campbell AJ et al (2005) Iron-rich silicates in the Earth's D″ layer. Proc Natl Acad Sci USA 102:9751–9753

Mao WL, Mao H-K, Sturhahn W, Zhao J, Prakapenka VB, Meng Y, Shu J, Fei Y, Memley RJ (2006) Iron-rich postperovskite and the origin of ultralow-velocity zones. Science 312:564–565

Masters G, Laske G, Bolton H, Dziewonski AM (2000) The relative behavior of shear velocity, bulk sound speed, and compressional velocity in the mantle: implications for chemical and thermal structure. In: Karato S-I, Forte AM, Liebermann RC, Masters G, Stixrude L (eds) Earth's deep interior: mineral physics and seismic tomography from the atomic to the global scale, Am. Geophys. Union, Washington, DC 63–87

Maupin V, Garnero EJ, Lay T, Fouch MJ (2005) Azimuthal anisotropy in the D″ layer beneath the Caribbean. J Geophys Res 110:10.1029/2004JB003506

McCammon C, Kantor I, Narygina O, Rouquette J, Ponkratz U, Sergueev I, Mezouar M, Prapenka V, Dubrovinsky L (2008) Stable intermediate-spin ferrous iron in lower-mantle perovskite. Nature Geosci 1:684–687

McNamara AK, Zhong S (2005) Thermochemical structures beneath Africa and the Pacific Ocean. Nature 437:1136–1139

Montelli R, Nolet G, Dahlen FA, Masters G (2006) A catalogue of deep mantle plumes: new results from finitefrequency tomography. Geochem Geophys Geosyst 11:doi:10.1029/2006GC001248

Mosenfelder JP, Asimow PD, Ahrens TJ (2007) Thermodynamic properties of Mg_2SiO_4 liquid at ultra-high pressures for shock measurements to 200 GPa on forsterite and wadsleyite. J Geophys Res 112:B06208. doi:10.1029/2006JB004364

Murakami M, Hirose K, Kawamura K, Sata N, Ohishi Y (2004) Post-perovskite phase transition in MgSiO3. Science 304:855–858

Murakami M, Hirose K, Sata N, Ohishi Y (2005) Post-perovskite phase transition and mineral chemistry in the pyrolitic lower mantle. Geophys Res Lett 32:doi:101029/2004GL021956

Nishio-Hamane D, Yagi T (2009) Equations of state of postperovskite phases in the $MgSiO_3$-$FeSiO_3$-$FeAlO_3$-system. Phys Earth Planet Int 175:145–150

Nishio-Hamane D, Nagai T, Fujino K, Seto Y, Takafuji N (2005) Fe^{3+} and Al solubilities in $MgSiO_3$ perovskite: implication of the $Fe^{3+}AlO_3$ substitution in $MgSiO_3$ perovskite at the lower mantle condition. Geophys Res Lett 32:doi:101029/2005GL023529

Nishio-Hamane D, Seto Y, Fujino K, Nagai T (2008) Effect of $FeAlO_3$ incorporation into $MgSiO_3$ on the bulk modulus of perovskite. Phys Earth Planet Int 166:219–225

Oganov AR, Ono S (2004) Theoretical and experimental evidence for a postperovskite phase of $MgSiO_3$ in Earth's D″ layer. Nature 430:445–448

Oganov AR, Ono S (2005) The high-pressure phase of alumina and implications for the Earth's D″ layer. Proc Nat Acad Sci 102:10828–10831

Ohta K, Hirose K, Lay T, Sata N, Ohishi Y (2008) Phase transitions in pyrolite and MORB at lowermost mantle conditions: implications for a MORB-rich pile above the core-mantle boundary. Earth Planet Sci Lett 267:107–117

Ohtani E, Sakai T (2008) Recent advances in the study of mantle phase transitions. Phys Earth Planet Int 170:240–247

O'Neil J, Carlson RW, Francis D, Stevenson RK (2008) Neodymium-142 evidence for Hadean mafic crust. Science 321:1828–1831

O'Nions RK, Evensen NM, Hamilton PJ (1979) Geochemical modeling of mantle differentiation and crustal growth. J Geophys Res 84:6091–6101

Ono S (2008) Experimental constraints on the temperature profile in the lower mantle. Phys Earth Planet Int 170:240–247

Ono S, Ohishi Y (2005) In situ X-ray observation of phase transformations in Fe_2O_3 at high pressures and high temperatures. J Phys Chem Solids 66:1714–1720

Ono S, Oganov AR (2005) In situ observations of phase transition between perovskite and $CaIrO_3$-type phase in $MgSiO_3$ and pyrolitic mantle composition. Earth Planet Sci Lett 236:914–932

Ono S, Ito E, Katsura T (2001) Mineralogy of subducted basaltic crust (MORB) from 25 to 37 GPa, and chemical heterogeneity of the lower mantle. Earth Planet Sci Lett 190:57–63

Ono S, Ohishi Y, Isshiki M, Watanuki T (2005) In situ X-ray observations of phase assemblages in peridotite and basalt compositions at lower mantle conditions: Implications for density of subducted oceanic plate. J Geophys Res 110:10.1029/2004JB003196

Ozawa H, Hirose K, Mitome M, Bando Y, Sata N, Ohishi Y (2008) Chemical equilibrium between ferropericlase and molten iron to 134 GPa and implications for iron content at the bottom of the mantle. Geophys Res Lett 35:L05308

Richards MA, Hager BH (1984) Geoid anomalies in a dynamic Earth. J Geophys Res 89:5987–6002

Richards MA, Engebretson DC (1992) Large-scale mantle convection and the history of subduction. Nature 355:437–440

Richards MA, Ricard Y, Lithgow-Bertelloni C, Spada G, Sabadini R (1997) An explanation for Earth long-term rotational stability. Science 275:372–375

Ritsema J (2005) Global seismic structure maps. In: Foulger GR, Natland JH, Presnall DC, Anderson DL (eds) Plates, plumes and paradigms. Geol Soc Am Spec Pap 388:11–18

Rost S, Garnero EJ, Williams Q, Manga M (2005) Seismic constraints on a possible plume root at the core-mantle boundary. Nature 435:666–669

Schersten A, Elliot T, Hawkesworth C, Norman M (2004) Tungsten isotope evidence that mantle plumes contain no contribution from the Earth's core. Nature 427:234–237

Shim S-H (2008) The postperovskite transition. Ann Rev Earth Planet Sci 36:569–588

Shim S-H, Bengtson A, Morgan D, Sturhahn W, Catalli K, Zhao J, Lerche M, Prakapenka V (2009) Electronic and magnetic structures of thed postperovskite-type Fe2O3 and implications for planetary magnetic records and deep interiors. Proc Nat Acad Sci 106:5508–5512

Sidorin I, Gurnis M, Helmberger DV (1999) Evidence for a ubiquitous seismic discontinuity at the base of the mantle. Science 286:1326–1331

Sinmyo R, Hirose K, O'Neill HSC, Okunishi E (2006) Ferric iron in Al-bearing postperovskite. Geophys Res Lett 33:L12S13

Sinmyo R, Hirose K, Nishio-Hamane D, Seto Y, Fujino K, Sata N, Ohishi Y (2008) Partitioning of iron between perovskite/postperovskite and ferropericlase in the lower mantle. J Geophys Res 113: doi:10.1029/2008JB005730

Sobolev AV, 19 co-authors (2007) The amount of recycled crust in sources of mantle-derived melts. Science 316:412–417

Stackhouse S, Brodholt JP, Price GD (2005a) High temperature elastic anisotropy of the perovskite and postperovskite polymorphs of Al_2O_3. Geophys Res Lett 32:L13305

Stackhouse S, Brodholt JP, Wookey J, Kendall J-M, Price GD (2005b) The effect of temperature on the seismic anisotropy of the perovskite and postperovskite polymorphs of $MgSiO_3$. Earth Planet Sci Lett 230:1–10

Stixrude L (1997) Structure and sharpness of phase transitions and mantle discontinuities. J Geophys Res 102:14835–14852

Stixrude L, Karki B (2005) Structure and freezing of $MgSiO_3$ liquid in Earth's lower mantle. Science 310:297–299

Stixrude L, de Koker N, Sun N, Mookherjee M, Karki B (2009) Thermodynamics of silicate liquids in the deep Earth. Earth Planet Sci Lett 278:226–232

Steinberger B, Torsvik TH (2008) Absolute plate motions and true polar wander in the absence of hotspot tracks. Nature 452:620–623

Stølen S, Trønnes RG (2007) The The perovskite to post-perovskite transition in $CaIrO_3$: clapeyron slope and changes in bulk and shear moduli by density functional theory. Phys Earth Planet Int 164:50–62

Takafuji N, Hirose K, Mitome M, Bando Y (2005) Solubilities of O and Si in liquid iron in equilibrium with (Mg, Fe)SiO3 perovskite and the light elements in the core. Geophys Res Lett 32:6313

Tateno S, Hirose K, Sata N, Ohishi Y (2005) Phase relations in $Mg_3Al_2Si_3O_{12}$ to 180 GPa: effect of Al on postperovskite phase transition. Geophys Res Lett 32:L15306

Tateno S, Hirose K, Sata N, Ohishi Y (2009) Determination of the post-perovskite phase transition boundary up to 4400 K and implications for thermal structure in D″ layer. Earth Planet Sci Lett 277:130–136

Thomas C, Kendall J, Lowman J (2004a) Lower-mantle seismic discontinuities and the thermal morphology of subducted slabs. Earth Planet Sci Lett 225:105–113

Thomas C, Garnero EJ, Lay T (2004b) High-resolution imaging of lowermost mantle structure under the Cocos plate. J Geophys Res 109:B08307

Tolstikhin I, Hofmann AW (2005) Early crust on top of the Earth's core. Phys. Earth Planet Int 148:109–130

Tolstikhin IN, Kramers JD, Hofmann AW (2006) A chemical Earth model with whole mantle convection: the importance of a core—mantle boundary layer (D″) and its early formation. Chem Geol 226:79–99

Torsvik TH, Smethurst MA, Burke K, Steinberger B (2006) Large Igneous Provinces generated from the margins of the large low-velocity provinces in the deep mantle. Geophys J Int 167:1447–1460

Torsvik TH, Smethurst MA, Burke K, Steinberger B (2008a) Long term stability in deep mantle structure: evidence from the ca 300 Ma Skagerrak-Centered Large Igneous Province (the SCLIP). Earth Planet Sci Lett 267:444–452

Torsvik TH, Steinberger B, Cocks LRM, Burke K (2008b) Longitude: linking Earth's ancient surface to its deep interior. Earth Planet Sci Lett 276:273–282

Trønnes RG, Frost DJ (2002) Peridotite melting and mineral-melt partitioning of major and minor elements at 22–24.5 GPa. Earth Planet Sci Lett 197:117–131

Tsuchiya T, Tsuchiya J (2006) Effect of impurity on the elasticity of perovskite and postperovskite: velocity contrast across the postperovskite transition in $(Mg,Fe,Al)(Si,Al)O_3$. Geophys Res Lett 33:L12S04

Tsuchiya T, Tsuchiya J, Umemoto K, Wentzcovitch RM (2004) Phase transition in $MgSiO_3$ perovskite in the earth's lower mantle. Earth Planet Sci Lett 224:241–248

Upadhyay D, Scherer EE, Mezger K (2009) ^{142}Nd evidence for an enriched Hadean reservoir in cratonic roots. Nature 459:1118–1121

van der Hilst RD, Karason H (1999) Compositional heterogeneity in the bottom 1000 kilometers of Earth's mantle: toward a hybrid convection model. Science 283:1885–1888

van der Hilst RD, de Hoop MV, Wang P, Shim S-H, Ma P, Tenorio L (2007) Seismostratigraphy and thermal structure of Earth's core-mantle boundary region. Science 315:1813–1817

van Keken PE, Hauri EH, Ballentine CJ (2002) Mantle mixing: the generation, preservation, and destruction of chemical heterogeneity. Ann Rev Earth Planet Sci 30:493–525

Vanpeteghem CB, Angel RJ, Ross NL, Jacobsen SD, Dobson DP, Litasov KD, Ohtani E (2006) Al, Fe substitution in the MgSiO3 perovskite structure: a single-crystal X-ray diffraction study. Phys Earth Planet Int 155:96–103

Walter MJ, Kubo A, Yoshino T, Brodholt J, Koga KT, Ohishi Y (2004) Phase relations and equation-of-state of aluminous Mg-silicate perovskite and implications for Earth´s lower mantle. Earth Planet Sci Lett 222:501–516

Walter MJ, Trønnes RG, Armstrong LS, Lord OT, Caldwell WA, Clarke SM (2006) Subsolidus phase relations and perovskite compressibility in the system $MgO\text{-}AlO_{1.5}\text{-}SiO_2$ with implications for the Earth's lower mantle. Earth Planet Sci Lett 248:77–89

Wookey J, Kendall, JM (2007) Seismic anisotropy and the lowermost mantle. In: Hirose K, Brodholt J, Lay T, Yuen D (eds) Post-perovskite. The last mantle phase transition. Am Geophys Union Geophys Monogr 174:171–189

Wookey J, Stackhouse S, Kendall JM, Brodholt J, Price D (2005) Efficacy of the post-perovskite phase as an explanation for the lowermost-mantle seismic properties. Nature 438:1004–1007

Yamazaki D, Yoshino T, Ohfuji H, Ando J-I, Yoneda A (2006) Origin of seismic anisotropy in the D″ layer inferred from shear deformation experiments on postperovskite phase. Earth Planet Sci Lett 252:372–378

Zerr A, Diegler A, Bohler R (1998) Solidus of Earth's deep mantle. Science 281:243–246

Zhang F, Oganov AR (2006a) Mechanisms of Al^{3+} incorporation in $MgSiO_3$ postperovskite at high pressures. Earth Planet Sci Lett 248:54–61

Zhang F, Oganov AR (2006b) Valence state and spin transitions of iron in Earth's mantle silicates. Earth Planet Sci Lett 249:436–443

Zhang JZ, Herzberg C (1994) Melting experiments on anhydrous peridotite KLB-1 from 5 to 22.5 GPa. J Geophys Res 99:17729–17742